Optical Test Stand and SiPM characterisation studies

von

Benjamin Glauß

Masterarbeit in Physik

vorgelegt der

Fakultät für Mathematik, Informatik und
Naturwissenschaften der RWTH Aachen

im Mai 2012

angefertigt im

III. Physikalischen Institut A

bei

Prof. Dr. Thomas Hebbeker

Abstract This thesis deals with developing and commissioning a test stand for optical SiPM characterisations. SiPMs are semiconductor-based photon detectors, said to become the classical photomultiplier tube's (PMT) successor in certain disciplines, where an SiPM's characteristics seem superior than these of a PMT. The test stand development is based on a given concept, that was devised in the previous bachelor theses [13] and [14]. The two main aspects in this thesis is on the one hand to complete the optics part and on the other hand to incorporate first example SiPM measurements. At the end, there is a solid basis given for complete SiPM characterisation studies, combining separate measurements in a single table-top setup, operating automatically with as little user interaction as possible, run by shell scripts.

Zusammenfassung Diese Arbeit setzt sich mit der Entwicklung und Inbetriebnahme eines Teststandes zur optischen Charakterisierung von SiPMs auseinander. SiPMs sind auf Halbleitermaterial basierende Photondetektoren, die in einigen Bereichen die klassischen Photomultipliertubes (PMTs) ersetzen werden auf Grund vorteilhafter Eigenschaften gegenüber PMTs. Die Entwicklung des Teststandes basiert auf einem bestehenden Konzept, das in den vorangegangenen Bachelorarbeiten [14] und [13] ausgearbeitet wurde. Die beiden Schwerpunkte dieser Arbeit liegen einerseits auf der Vervollständigung des Optikteils und andererseits der Aufnahme von Daten eines Test-SiPMs. Am Ende steht eine zuverlässige Lösung für komplette SiPM Charakterisierungen, welche bisher separate Messungen in einem einzigen, kompakten Aufbau zusammenfasst und automatisch mit so wenig Eingreifen des Benutzers durch autarke Shell-Skripte abläuft.

Contents

1. An Introduction to SiPMs and their Properties 1

2. Teststand Concept 9
   - 2.1. Optics . . . 10
     - 2.1.1. Light Sources . . . 12
     - 2.1.2. Light Propagation . . . 15
     - 2.1.3. Optical Measurements . . . 20
   - 2.2. Devices . . . 21

3. SiPM Characterisation 27
   - 3.1. Principle of Measurements . . . 27
   - 3.2. Pre-Characterisation . . . 27
     - 3.2.1. I-V-Line . . . 29
     - 3.2.2. 0.5 P.E. Threshold Determination . . . 31
     - 3.2.3. Breakdown Voltage Determination . . . 33
     - 3.2.4. Photon Equivalent Peak Width . . . 36
   - 3.3. Photon Detection Efficiency . . . 38
     - 3.3.1. Relative Photon Detection Efficiency . . . 40
     - 3.3.2. Absolute Photon Detection Efficiency . . . 43

4. Summary and Conclusion 51

5. Outlook 53

Bibliography 55

A. Abbreviations 59

B. Additional Figures 61

1. An Introduction to SiPMs and their Properties

The Silicon Photomultiplier (SiPM, cf. Fig. 1.1) is a semiconductor-based detector developed for counting photons in the wavelength range between 320 nm up to 900 nm with a peak sensitivity at 440 nm [1]. This means that the SiPM is aiming at becoming the successor of the Photomultiplier Tube (PMT). PMTs are used in several important high-energy particle physics experiments such as the CMS experiment at LHC/CERN, where it is used to detect photons in the hadron forward (HF) region of the hadron calorimeter, or in the Auger experiment in Argentina, where PMTs detect fluorescence light from air showers ([2], [3]).

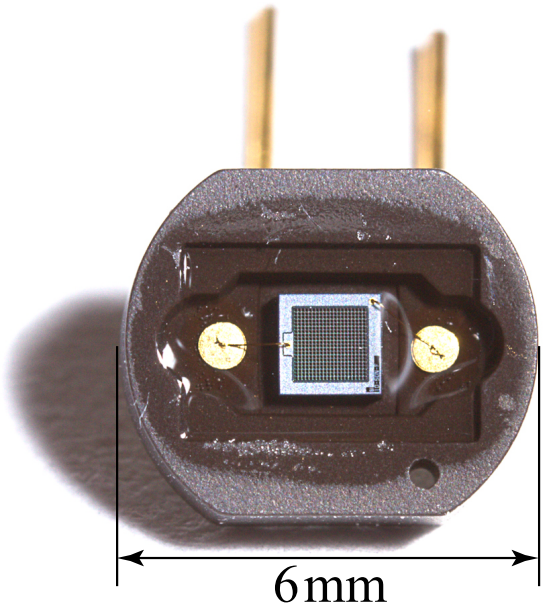

Figure 1.1.: A Hamamatsu SiPM, Model S10362-100C with 900 pixels and $(1\text{x}1)\ \text{mm}^2$ active area (Photo: Benjamin Glauß, 2012).

Currently, the collaborations of the experiments mentioned are working on upgrade plans, that show how SiPMs can be incorporated into these experiments

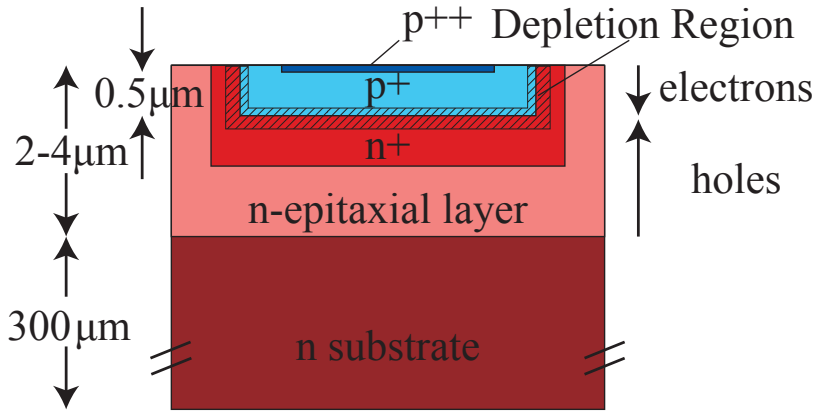

Figure 1.2.: Simplified schematic depiction of a p-on-n type G-APD (Benjamin Glauß, 2012).

([4], [5]). SiPMs are considered better to use in some circumstances due to their smaller size, lower operating voltage and insensitivity towards magnetic fields compared to PMTs. Furthermore, they have a higher photon detection efficiency (p.d.e.). SiPMs are well-suited for mass production and can be easily tailored to specific needs concerning the adjustment of semiconductor parameters (i.e. p-on-n or n-on-p, thickness of depletion region -> impacts on wavelength sensitivity; resistor types -> influencing temperature dependence) [6]. The SiPM itself consists of single micro-cells or pixels arranged in a pattern that is for example quadratic. These cells have a width (pitch) and a fill factor (ratio between the pixel's light sensitive region to its whole surface). This SiPM surface containing the light sensitive pixels is behind a protective window that has a negligible absorption in the visible regime. An SiPM's connection is established through two connectors, an anode and a cathode. Via these, the SiPM is supplied with an operating voltage and also the signals due to incident photons can be passed on to an amplifier.

The basic functional principle of SiPMs is similar to that of a solar cell. This means that there are differently doped silicon-based layers (p-n-junction) to which a *bias voltage* V_{bias} is applied and thus a depletion region of width

$$d = \sqrt{\frac{2\varepsilon_{\text{SI}}}{e} \cdot \frac{N_{\text{A}} + N_{\text{D}}}{N_{\text{A}} N_{\text{D}}} \cdot V_{\text{bias}}}$$

$$d \approx \sqrt{\frac{2\varepsilon_{\text{SI}}}{e} \cdot \frac{1}{N_{\text{D}}} \cdot V_{\text{bias}}} \text{ ([10], p.20)}$$

is created, with the approximation to have an one-sided abrupt junction, i.e. the number of acceptors N_A is much larger than the number of donators N_D. ε_{SI} is the permittivity in silicon, e is the elementary charge.
The bias voltage is

$$V_{bias} = V_{OV} + V_{BD}, \tag{1.1}$$

the sum of *over voltage* V_{OV}, applied to the SiPM additional to its *breakdown voltage* V_{BD}, giving the voltage at which the SiPM operates in Geiger mode and avalanches are released for created pairs of charger carriers (electron-hole pair). Furthermore, V_{BD} itself depends on temperature and can be written as

$$V_{BD} = V_{B0} \cdot [1 + \beta \cdot (T - T_0)] \text{ ([6], p.29)},$$

where V_{B0} is a reference value at a given temperature T_0 and β is the temperature coefficient, describing the change of V_{BD} with changing temperature T.
A photon being incident to this region creates a charge carrier pair. In silicon, the amount of energy needed is equal to 1.12 eV that corresponds to a wavelength of 1100 nm. The pixel type shown in Fig. 1.2 is a p-on-n-type junction, that is the junction of our choice for detecting high energetic photons in the blue until near UV regime of the electromagnetic spectrum rather than a n-on-p type which is suited for red/infrared light detection. Also, the width of the depletion region has to be adjusted to the photons' absorption length, that varies for different wavelengths. In the near UV regime, this is only about 10 nm. The incident photon gives rise to an avalanche in one single SiPM pixel due to the pixel's electronic characteristics, depicted in Fig. 1.3. As can be seen, a single SiPM pixel is an avalanche photodiode, operated in Geiger mode (hence a Geiger mode avalanche photo diode, G-APD), i.e. above its avalanche breakdown voltage. The avalanche causes a high gain that can be derived from

$$G = (V_{bias} - V_{BD}) \cdot C_{pixel}/e \text{ [7]}, \tag{1.2}$$

where C_{pixel} is a pixel's capacitance and q_0 the elementary charge, where C_{pixel} has typical values of $10 - 100$ fF and is quite uniform distributed with $\sigma_1/S_1 \simeq 10\,\%$. Typical gains are $G \approx 10^6$. This high gain is the reason for an SiPM to have a very low intrinsic electronic noise.
The avalanche has to be stopped, in this case by a *quenching resistor* R_q operated in series, shown in the electric model for one single pixel (Fig. 1.3) that also

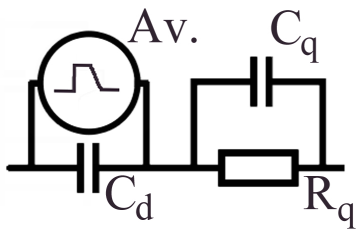

Figure 1.3.: Electric scheme for a single SiPM pixel denoting the components that account for a pixel's electrical behaviour (Benjamin Glauß, 2012).

Figure 1.4.: Size comparison between a Photomultiplier Tube on the left and the SiPM as in Fig. 1.1 (Photo: Benjamin Glauß, 2012).

includes the *quenching capacitance* C_q, the *diode capacitance* C_d and a symbol for the avalanche itself. The avalanche discharges the pixel from the bias voltage until its breakdown voltage. Eventually the pixel is quenched and recharged until it reaches its operating voltage again, giving rise to a dead time until full recharge of the pixel.

The pixel array can be built with a high pixel-to-pixel accuracy, that the amount of electrons released at each breakdown is every time approximately equal for the same input amount of light, resulting in an excellent photo-electron resolution. The outcome is the capability of detecting signals of single photons. The new technology SiPMs are based on certainly brings advantages, of which some are for example a reduced size (from several tens of centimeters for PMTs to some millimeters, cf. Fig. 1.4), though a PMT's sensitive area is larger and reduced

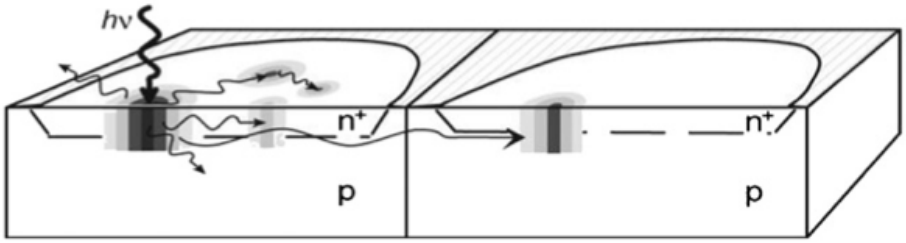

Figure 1.5.: Schematic depiction of a crosstalk event in two neighbour cells [8].

operating voltage (a kilovolt to only a few tens of volts). Another important advantage is the higher p.d.e. an SiPM can offer. Also, SiPMs are insensitive to magnetic fields. On the other hand there are disadvantages as well that need to be understood and quantised before SiPMs can be utilised in experiments.

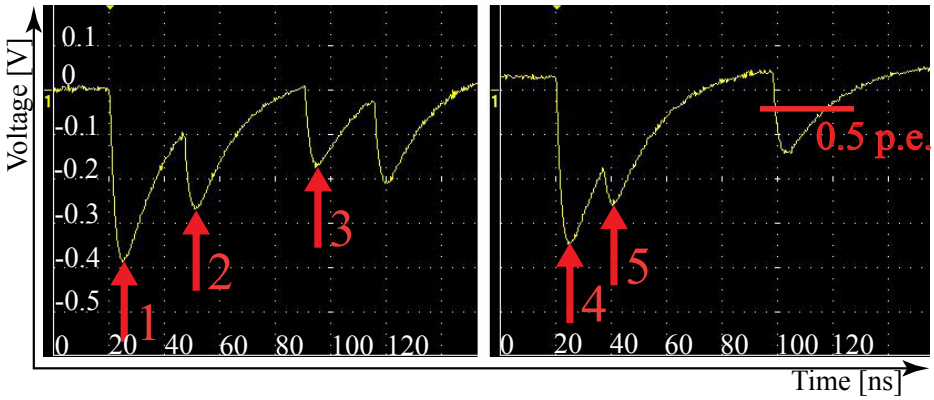

Figure 1.6.: SiPM pulses showing different effects and an example for a 0.5 p.e. pulse height. The scope's resolution is set to 100 mV/div, the time resolution is set to 20 ns/div.

The disadvantages compared to PMTs include especially noise phenomena such as the temperature-dependent *dark noise*, *afterpulsing* and *optical crosstalk* and hence the SiPM's p.d.e. has to be corrected for these effects [9]. Optical crosstalk is produced through photons that are created in an avalanche and escape the pixel, inducing another Geiger discharge in a neighboring pixel (cf. Fig. 1.5). Optical crosstalk can be reduced by setting trenches between the pixels, shielding neighboring pixels. Afterpulsing originates from avalanche charge carriers being temporarily trapped in the semiconductor's impurities and can trigger new avalanches themselves after a certain time delay, faking an incident photon. The latter effect can reach levels of 1 kHz to 1 MHz when setting a trigger threshold at the oscillo-

scope to a voltage equivalent the 0.5 photon equivalent peak pulse height (cf. Fig. 1.6, even though the signals are negative, they are considered being peaks), i.e. to the value according to half the height that one single incident photon would cause. A scope signal produced by an SiPM can be seen in Fig. 1.6. This was recorded having an SiPM attached to an inverting amplifier, the detailed configuration can be taken from chapter 2.2. The signals shown are for explanatory reasons only, and the statements given are probable interpretations. Peak 1 shows a signal that is due to two firing pixels, compared to signal 3, that has only half the height of signal 1. Hence signal 3 corresponds to one firing pixel. Signal 2 that is sited on signal 1's tail is another full height single cell signal due to another pixel that fired shortly after signal 1. Signal 4 is the same as signal 1, but in this case signal 5 is not another firing cell, but it might be caused by afterpulsing (note that the signal on the rising edge does not have the full height as signal 3, due to the fact that the pixel has not been fully recharged yet). The signals were recorded with a scope at time division 50 ns and voltage division 200 mV.

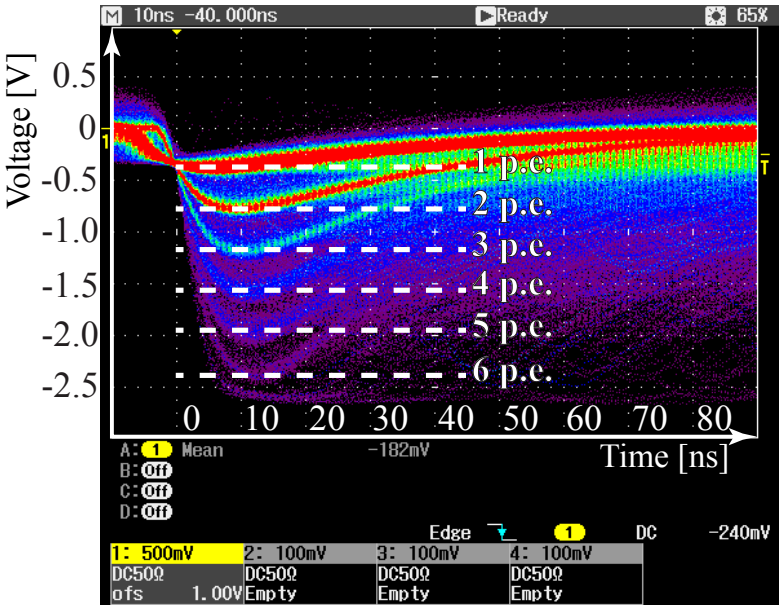

Figure 1.7.: Different SiPM pulses heights, representing the different charge amounts released in a breakdown for 1, 2, 3,... pixels. The trigger level is set to $V_T = -240$ mV.

Figure 1.7 shows a scope image that has recorded SiPM signals over a minute with infinite persistence time. The different heights shown are due to the number of cells firing at the same time and are called photon equivalent (p.e.), the smallest being the 1 p.e.

An SiPM's p.d.e. depends on three quantities that are the fill factor $\epsilon_{\text{geometry}}$, the Geiger discharge probability ϵ_{Geiger} that gives the probability that the created electron-hole pair triggers an avalanche breakdown and the quantum efficiency:

$$p.d.e. = QE \cdot \varepsilon_{\text{Geiger}} \cdot \varepsilon_{\text{geometry}} \; [7]. \tag{1.3}$$

Corrections for the noise phenomena mentioned would give an effective p.d.e. significantly lower than shown in Fig. 1.8 as we will see later on in this thesis. This justifies the need of characterising SiPMs to get reliable values, since some manufacturers claim their SiPMs are capable of 74% p.d.e. in a given regime.

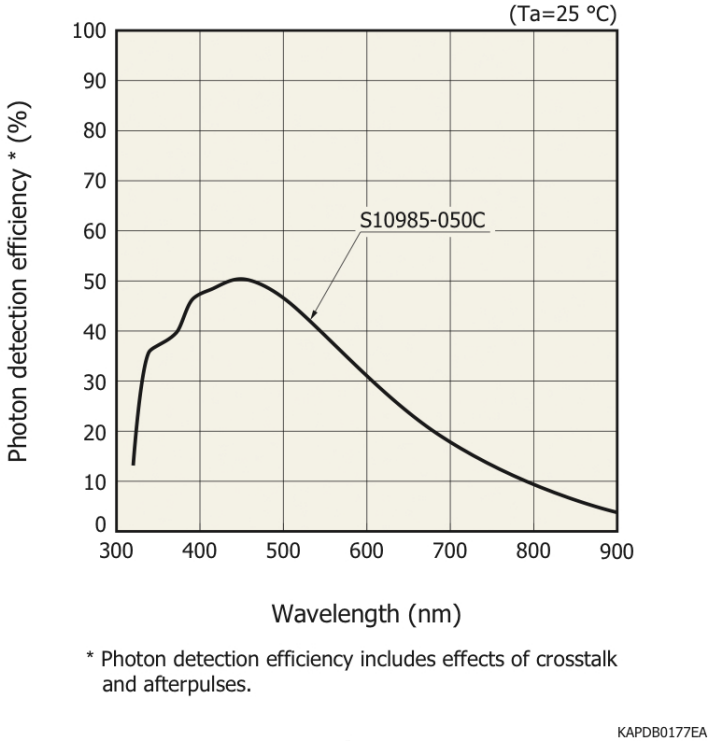

Figure 1.8.: P.d.e. for a Hamamatsu Silicon Photomultiplier [1].

Another characteristic to be understood is an SiPM's linearity. For a number of incident photons significantly lower than the amount of pixels, and in case of saturation the SiPM's signal is linear and can be described by

$$N_{\text{signal}} = N_{\text{pixels}} \cdot \left(1 - e^{\text{p.d.e.} \cdot N_{\text{photons}}/N_{\text{pixels}}}\right) \; [7],$$

for an N_{signal} p.e. signal height. A further noise component is temperature-dependent dark noise, that is due to thermally generated charge carriers and can reach several 100 kHz at room temperature.

2. Teststand Concept

SiPMs feature a lot of properties which were presented in section 1. These themselves depend on the operating voltage and on the ambient temperature. Each of the following characterisation measurements has to be performed as a function of those two quantities:

Characteristics And Measurements	
Pre Characterisation	I-V-Line 0.5 p.e. Equivalent Breakdown Voltage Absolute Gain
p.d.e.	Relative (Continuous light flux) Absolute (Pulsed light flux)
Noise	Dark Noise Afterpulsing Optical Crosstalk
	Linearity Recovery Time

Table 2.1.: Characteristics to be measured with the test stand once completed.

To learn more about the single measurements, the reader might consider studying the work of Markus Lauscher [10] and Patrick Hallen [15].
Carrying out the above each one after the other is obviously very time consuming and the main reason why to integrate these into one automised setup. Further requirements to this setup are to deliver reliable results despite the required time efficiency and to be small in dimensions, i.e. not to be larger than a desk for example. Other thoughts that influenced the overall setup idea was to have the possibility of testing the SiPM wavelength dependent with a focus on wavelengths in the visible regime and the near UV regime. As will be shown, a very good wavelength resolution has been achieved, so that narrow lines from the electromagnetic spectrum can be used for characterising the SiPMs. The two main parts, the optics table and the automisation devices will be explained individually in the following chapters.

2.1. Optics

The optic table consists of a few main components:

- Light Sources
- Acrylic Cone Condensor
- Collimator
- Optical Fibers
- Reflective Grating
- Movable Light Pickup
- Integrating Sphere
- Neutral Density Filter

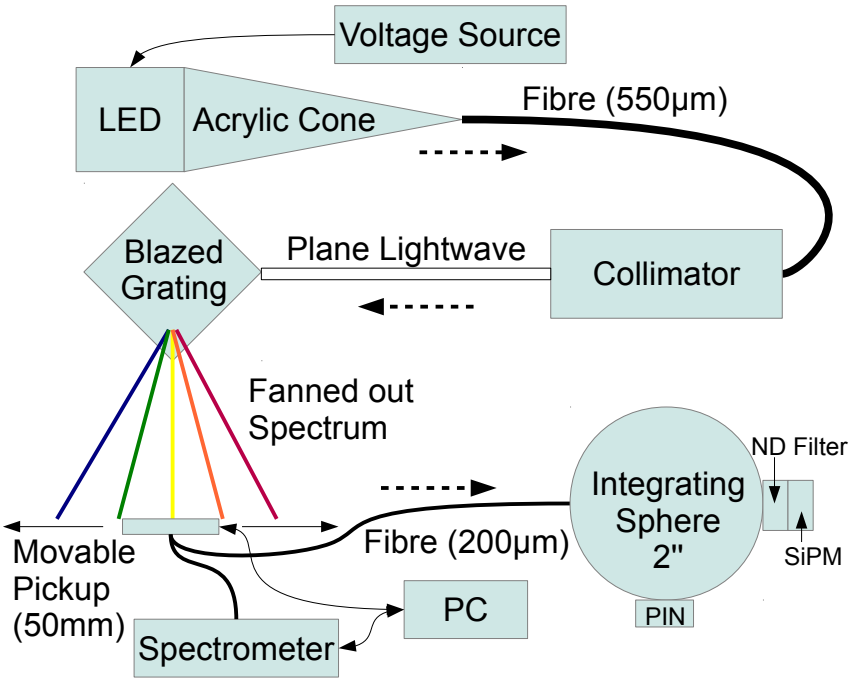

Figure 2.1.: Schematic depiction of the light from the source being fanned out in the monochromator and coupled into the integrating sphere.

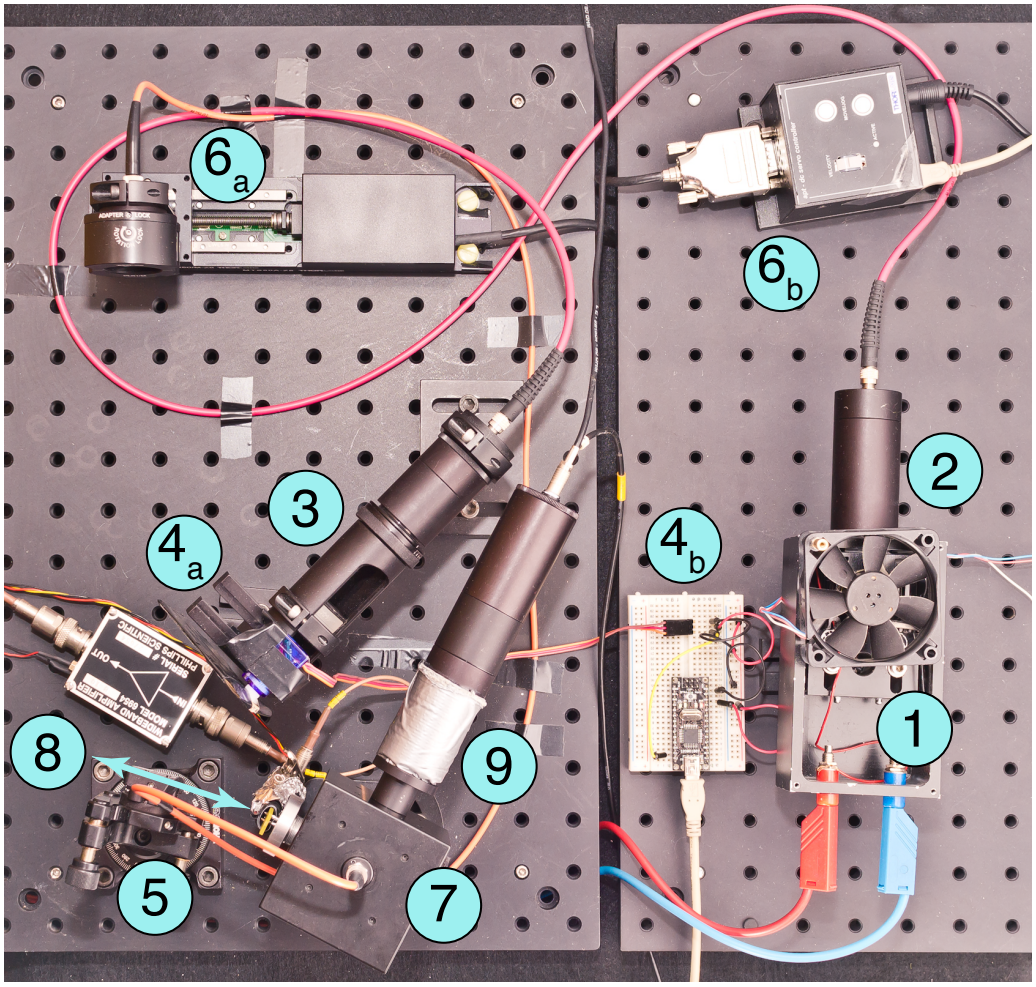

Figure 2.2.: Photograph of the optic table, showing the different components. The white LED is at position 1. The cone is inside the black tube at 2. The condenser is inside the tubes at 3. A shutter to screen the light is attached to the condenser tube at 4 a and controlled by a microchip at 4 b. The grating is at position 5. The pickup is at 6 a and moved by a DC servo motor at 6 b. The integrating sphere is at 7, where the SiPM (8) and the PIN diode are attached to.

In Fig. 2.1 the components and their order is shown, see Fig. 2.2 for a photograph of the setup. Beginning at the light source, its light is coupled into the first fibre (diameter: 550 µm) through an acrylic cone that functions as a light concentrator. In a two lens collimator, the light from the first fibre is turned into a plane wave and directed onto a reflective grating, that fans out the white light. A pickup (fibre with diameter 200 µm) is mounted on a motorised stage and can pick up light at different positions and hence wavelengths, which is either coupled into an integrating sphere or into a spectrometer. The purpose for the latter is to calibrate

wavelengths vs. pickup position. Detailed explanations why those components were chosen and how measurements were carried out are presented below. The components where light passes through were chosen in such kind of way, that these are also transparent to light below 400 nm. These are the acrylic cone, the collimator lenses and the fibres. Curves can be found in Fig. B.10 through B.13

2.1.1. Light Sources

The two light sources are used to measure the SiPM's p.d.e. In both cases, different light emitting diodes (LEDs) are used. To measure the relative and absolute p.d.e. values as a function of wavelength, one needs a constant light source (white LED) for relative p.d.e. measurements and pulsed LEDs for the absolute p.d.e. The reason for this is, that the current through the SiPM is proportional to the relative p.d.e. at a given wavelength, but for an absolute (p.d.e.) scale, one needs to know how many photons in a single pulse were incident on the SiPM's surface. The white LED uses the light of a low-wavelength LED (blue, for example InGaN) that is covered by a phosphorous substance (YAG:Ce^{3+}). The light emitted by the LED can partially pass through the phosphorous material unchanged, whereas a fraction undergoes stokes shift and is broadened (see Fig. 2.3). Stokes shift is caused by the energy loss due to rotational excitation of the molecule that has absorbed the blue LED's photon.
With this technique, it is possible to create a light source that emits light in a broad regime of the visible spectrum, even though it is still not homogeneous. Another drawback coming from the inherent characteristics of phosphorescent materials is the rather long decay time. YAG:Ce^{3+} has a decay time of <100 ns [16], that is still too much for the purposes absolute p.d.e. measurements require ($\sim$10 ns). The white LED used in the setup is a *Cree* CXA2011 with maximum power consumption of 44.9 W and a maximum luminous flux of 2610 lm. Since the LED generates a considerable amount of heat, it needs to be actively cooled. Furthermore it is important, that the LED is powered a while before measurements are recorded, since it needs to reach a equilibrium state. The light flux is measured with a PIN diode. A constant current measured, indicates a constant photon flux assuming that the spectrum does not vary. To have an estimator for that, Fig. 2.4 and B.1 show what happens when the LED is either switched on or the current is lowered (instantly from 0 mA to 800 mA, respectively from 700 mA to 600 mA). Decreasing the current, the LED cools down after a certain time and becomes more efficient. Due to the heat generation, a currency of 700 mA is chosen to

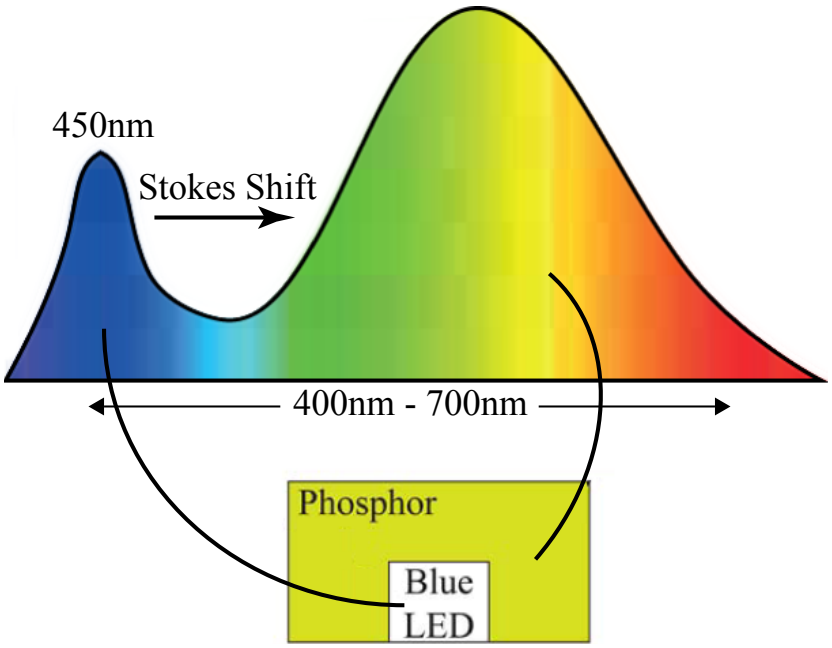

Figure 2.3.: White light LED consisting of short wavelength LED at the bottom surrounded by a phosphorous substance, the resulting white light LED's spectrum is shown above (Benjamin Glauß, 2012).

make sure that no overheating is the case.

Increasing the current, the effect is the other way around, i.e. due to a larger amount of heat that is generated the LED loses efficiency. The setup for the measurements consists of the LED itself, the light is coupled via cone and fibre into the integrating sphere, and the current shown in the curves is the PIN current measured with a picoammeter. The current measured is proportional to the amount of photons reaching the PIN diode. Through fitting an exponential function to the data in Fig 2.4, a time constant τ of about 275 s is determined. It shows, that in every case one should wait approximately ten minutes before using the LED for measurements.

The light source used for absolute p.d.e. measurements can be seen in figure 2.5. The board was designed and manufactured in collaboration with our RWTH 3A electronics department. Its electric circuit can be found in the appendix (Fig. B.2). Seven LEDs with different wavelengths (table 2.2) are used, to measure absolute p.d.e.s over a large spectral range. Spectra for each single LED can be found in the appendix (Fig. B.3 through B.9). For the LEDs an impedance and voltage matching was carried out and the electric signals were checked at an oscilloscope when pulsing a LED. Each LED is in series with a transistor, that

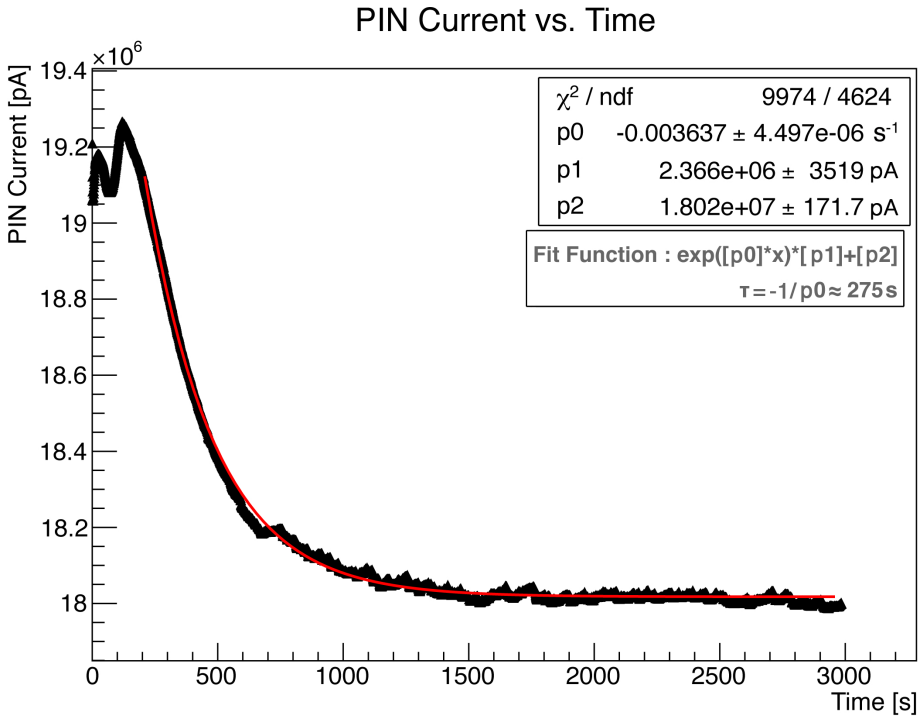

Figure 2.4.: At time $t = 0$ the white LED is switched on. The PIN diode measures a current (y-axis) that is proportional to the LED's light flux.

is used to switch the LED to operating or non-operating mode. The transistors themselves are controlled by an Arduino micro-controller board, supplying the base with the necessary voltage. This micro-controller is attached to a computer via USB so the LED to be operated can be chosen from within the programs used for measuring purposes. The electrical pulses used to flash the LEDs are generated with an arbitrary function generator (AFG3252), further described in chapter 2.2 that also triggers the measurements itself, hence measurements only take place when a LED was pulsed. Since the AFG can only supply the LED board with 5 V, an amplifier is attached to the LED board, that is to be operated with +12 V and -3 V. For later measurements, the LEDs 3, 4 and 5 are used, since they are able to generate enough light for the final setup for p.d.e. measurements in chapter 3.3. The LEDs' wavelengths cover the blue regime to adjust the relative white LED measurements to an absolute scale. The LEDs are also coupled into a fibre (1 mm diameter) through an acrylic cone.

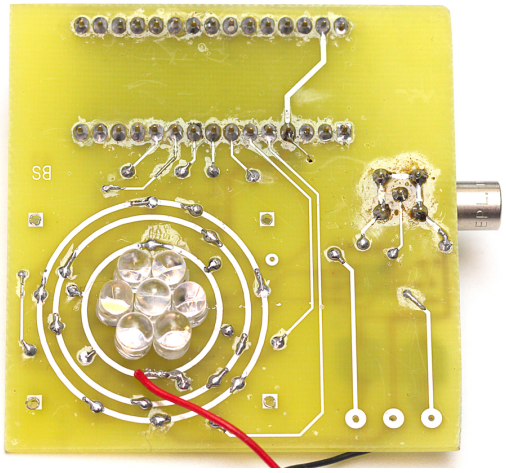

Figure 2.5.: LED board housing seven monochromatic LEDs, electric components and cabling for pulsed operation (Photo: Benjamin Glauß, 2012).

LED #	Mean wavelength [nm] (manufacturer)	Peak wavelength [nm] (measured)	FWHM [nm] (measured)
1	370	371.7	11.0
2	384	380.1	8.4
3	407	395.0	11.3
4	470	464.8	24.6
5	505	503.8	30.9
6	525	515.7	28.0
7	575	554.0	105.8

Table 2.2.: Properties of the seven LEDs for measuring absolute p.d.e.s.

2.1.2. Light Propagation

In the following, a description of the different stages the light propagates from the sources explained in chapter 2.1.1 until coupled into the integrating sphere is given. All the components used are either from *ThorLabs* or manufactured at the institute's workshop. The components that can be seen in the schematic depiction in Fig. 2.1 are attached on top of two breadboards[1] of which the one housing the the pickup, the collimator and the integrating sphere can be shielded from light by a dark box.

[1] ThorLabs model MB3045/M, dimensions: 300 mm x 450 mm x 12.7 mm

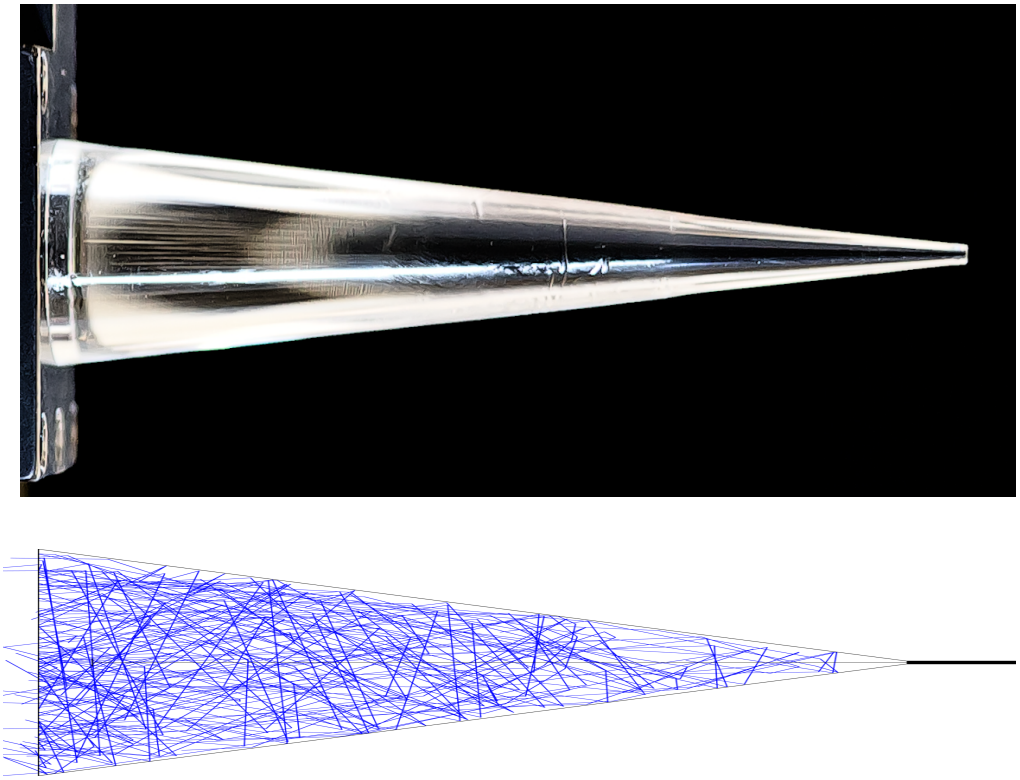

Figure 2.6.: Acrylic cone used to couple the different extended light sources into a fiber. Below is a simulated cone, done in Zemax (Photo: Benjamin Glauß, 2012).

Condensing

Since the different light sources used are not point like but rather extended (d $\approx$ 15 mm) (cf. chapter 2.1.1), different possibilities were studied to couple the sources' light into a light-guiding fiber. One possibility is to use a collimating system consisting of two convex lenses whose aperture are chosen in such a way that they are matching the light sources' and the fiber's diameter and numerical aperture. A further idea is to use a massive acrylic cone. Such a cone was simulated with the optic-simulation program *ZEMAX*[2], indicating a promising gain in light yield of a factor $\sim$10 over the lens system.

The acrylic cone was manufactured at the institute's mechanical workshop. The cone's characteristics were adjusted to the fibre's numerical aperture (cf. Eq. 2.1). The Cone's diameters are chosen to match the light sources' diameter [3] and

[2] http://www.radiantzemax.com/

[3] White LED $d_1 = 16.2$ mm, three LEDs adjacent to another $d_2 \approx 15$ mm, d_1 was eventually for the cone.

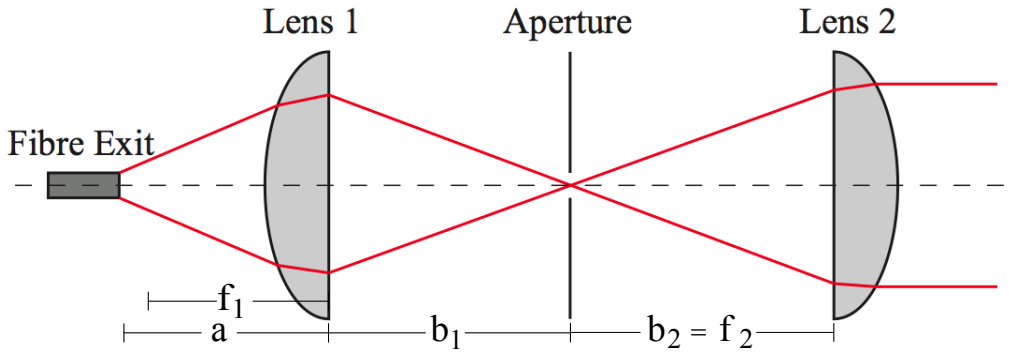

Figure 2.7.: Two stage collimator with an aperture, used to create a plane wave (Benjamin Glauß, 2012).

the fiber's diameter, respectively. Furthermore, adapters were lathed to fixate the cone inside of a 1" aperture tube that are used throughout the table to house the optical components. A photograph showing the used cone can be seen in Fig. 2.6.

Collimating

The light exiting the 550 µm diameter fibre (Fig. 2.1) is fanned out to be able to pick up different wavelengths. To be able to fan out the light, it is necessary to have a plane wave and parallel light rays incident on a blazed grating, further described in [13]. This step is called collimation and realized by two lenses in a lens tube, having an aperture in between. The first lens is used to create a focal point at the aperture, the second lens creates the plane wave (cf. Fig. 2.7).
The collimator design was carried out with respect to divergence minimisation, that is the main influence on the FWHM in the fanned out spectrum mentioned in 2.1.3 (cf. Fig. 2.9). This rest divergence Θ is due to the extended light source used (in this case the fibre end) and is inversely proportional to the focal length of lenses in use:

$$\begin{aligned} \Theta &\sim 1/f_{\text{net}} \\ f_{\text{net}} &= \frac{f_1 f_2}{f_1 + f_2 - d} \text{ ([17], p.78)} \end{aligned}$$

where $d = b_1 + b_2$ is the distance between the two lenses and $b_2 = f_2$ by definition, since we require a plane wave after lens 2, hence the distance between the lens

two and the crossing point of the light needs to be equal to the focal length of lens 2. For a given tube length ($a + b_1 + b_2 \approx 110\,\text{mm}$) the optimisation led to a net focal length of $f_{\text{net}} = 150\,\text{mm}$, consisting of two lenses with focal lengths $f_1 = 11\,\text{mm}$ and $f_2 = 40\,\text{mm}$. The different lengths are optimised with *Maple* and fine adjustments are carried out with the spectrometer attached to the movable pickup and the white LED switched on. During setup and calibration of the collimator, spectra are monitored in real time and the lens position is corrected with respect to the spectra's profile and light intensity. In front of the pickup, a cylindrical convex lens is attached with its curved surface directed towards the grating. This lens is used to focus the fanned out spectrum on a line where the pickup is located.

Fibres

The fibres in use to transport the light from the condensing cone to the collimator and from the light pickup into the integrating sphere are cladded light guides from *ThorLabs* which have an inner diameter of 550 µm and 200 µm respectively and both are equipped with standard SMA 905 optical connectors. Both fibers have a numeric aperture of 0.22, defined by

$$NA = n_{\text{air}} \cdot \sin\Theta_{\text{max}} = \sqrt{n^2_{\text{cladding}} - n^2_{\text{core}}}\ ([17], \text{p.106}), \tag{2.1}$$

where Θ_{max} is the fibre's maximum angle of acceptance, defined by the material constants, that are the refractive indices n_{core} and n_{cladding} of the fibre's core material and cladding, respectively. Due to the fibres' silica cores, it is important to pay attention not to have a too small bending radius, that would decrease the transmission. The recommended spectral range is 350 mm to 2200 nm, while having a transmission of above 95 % between 400 nm and 2100 nm, the material's attenuation curve can be found in B.13.

Neutral density filter

To decrease the amount of photons that reach the SiPM compared to the photon flux that reaches the PIN diode, a neutral density filter from ThorLabs is used that decreases the light intensity in the visible regime roughly to about ten percent (cf. Fig. B.14). This filter is mounted directly in between the SiPM and the integrating sphere to make sure the SiPM is not in saturation while the PIN diode is still illuminated sufficiently to measure significant currents above its dark noise. In order to know the wavelength dependent transmission factor, spectra are recorded

with a spectrometer, comparing the spectrum with the ND filter with a spectrum without the ND filter.

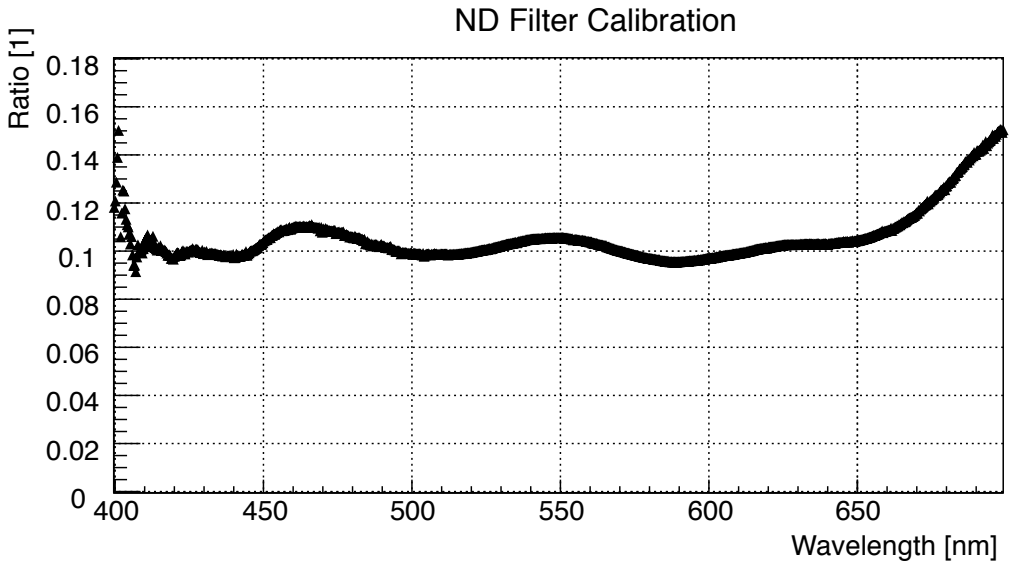

Figure 2.8.: Calibration data for the neutral density filter ND1.0.

These spectra are recorded with a setup as follows: The light source (white LED) is coupled into the integrating sphere via the acrylic cone and the 550 µm fibre. On another sphere port the neutral density (ND) filter is attached and a further 550 µm fibre picks up the light after passing through the filter and leads it into the USB spectrometer. A spectrum (S_{filter}) is recorded. In a second setup (spectrum S_{tube}), the ND filter is exchanged by a tube of the same length as the filter. A third measurement (spectrum S_{bg}) is carried out with the LED switched off, to correct for the background. For the measurement with the LED switched on, the LED is held at constant power of ~ 30 W. Spectra are recorded with a constant integration time, giving a maximum value adjusted to the spectrometer's resolution for the measurement without a filter and light switched on due to expecting highest intensities in this case. In total, 25 spectra are recorded for each of the three setups. Three mean spectra ($(\sum S_i)/25 = \bar{S}_i$) are computed through those. A ratio is determined subtracting the dark measurements from both measurements with and without filter, subsequently these are divided: $R = (\bar{S}_{\text{filter}} - \bar{S}_{\text{bg}})/(\bar{S}_{\text{tube}} - \bar{S}_{\text{bg}})$. Fig. 2.8 shows the resulting ratio vs. wavelength plot used to correct the photon flux for the wavelength dependent filter properties. The plot reflects the expectations given through Appendix B.14 reliably, but only for the region that has a sufficient photon flux due to the LED characteristics.

Integrating Sphere

To make the light diffuse before being incident on the SiPM, an integrating sphere from *ThorLabs* is used[4], uniformally scattering the incident light at a high reflectivity destroying the light source's spatial characteristics through multiple reflections and hence satisfying Lambert's cosine law. The different light sources are coupled into the integrating sphere and PIN diode and SiPM are attached to its ports. Spectrometer measurements are directly connected to the pickup, omitting the integrating sphere. The sphere is hollow with a highly reflective material (PTFE)[5] on its inside. More about integrating spheres for SiPM testing purposes can be found in [18].

2.1.3. Optical Measurements

In order to show the SiPMs' characteristics (as listed in Tab. 2.1) as wavelength-dependent functions, a calibration has to be carried out. This calibration translates the position of the movable pickup (cf. Fig. 2.1) into wavelengths, since only the pickup position can be accessed through the software controlling the pickup. The white LED is fanned out using the blazed grating. The spectrum is directed at the movable pickup, such that the spectrum approximately extends over the range of 50 mm. This is the distance, the pickup can move. At the light pickup position, another 200 µm fibre is placed, that conducts the light into a spectrometer. The pickup is moved five times along the whole 50 mm range in steps of 1 mm. At each position a spectrum is recorded. Fig. 2.9 shows an example spectrum at the absolute position of 44 mm. The maximum wavelength returned by the spectrometer at this position is 416.04 nm with a full width at half maximum of 5.78 nm.

The fibre spectrometer has a linear silicon CCD array with 650 pixels. Each pixel integrates photons and translates these into counts (1 count $\widehat{=}$ 75 photons at 400 nm) [19]. The integration time is dynamically adjusted by the software in use. The highest intensity is set in such a way, that the spectrometer's range is not exceeded. It is limited to 1000 ms, since the calibration is supposed to be not too time consuming. A dark spectrum is subtracted from each measured spectrum. For each of the five repetitions at a position, the maximum wavelength and the FWHM is determined. Eventually a mean value for each spectrum's maximum wavelength and FWHM is calculated. Fig. 2.10 shows the results

[4] Model IS 200

[5] See Fig B.15 for reflectivity characteristics

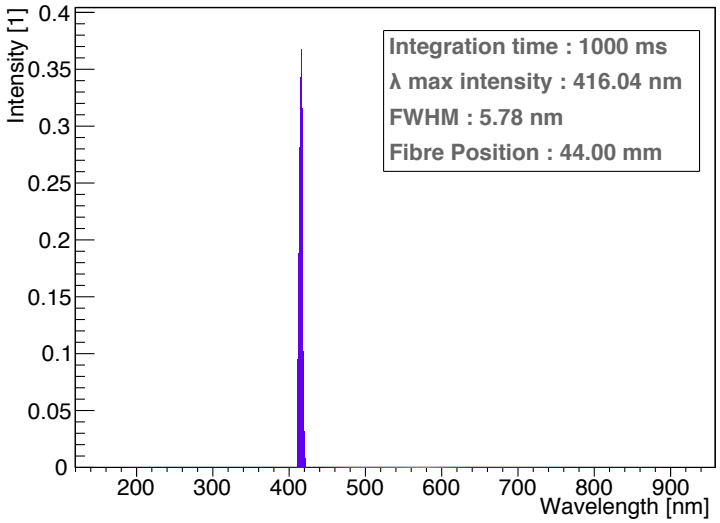

Figure 2.9.: Single spectrum recorded with the spectrometer for calibration purposes

for pickup position versus mean wavelength. A line is fitted to show the linear behaviour of the measurement. The relatively high normalised χ^2 value of about nine indicates that a linear correlation might not be the optimal assumption. This becomes obvious if one thinks for example, that the wavelength is not exactly fanned out on one line but rather on a circle segment. This is also indicated by the systematic deviation of the residue positions just below 40 mm, where the pickup is perpendicular to the post the grating is mounted on. For calibration purposes nevertheless the fit's parameters that are extracted are used. These will be further used to calculate wavelengths for each of the following measurements where table positions are accessed. The fit parameters are saved to a config file that is read by the programs analysing the p.d.e. in chapter 3.3. To have an estimator for how good the monochromator works, the spectra's FWHM are plotted against the wavelength, resulting in FWHM values constantly below 10 nm over the whole regime, with a better performance in the blue region (cf. Fig. 2.11).

2.2. Devices

The following paragraphs will give an overview of the devices used either for voltage supply or for the different SiPM characterisation measurements.

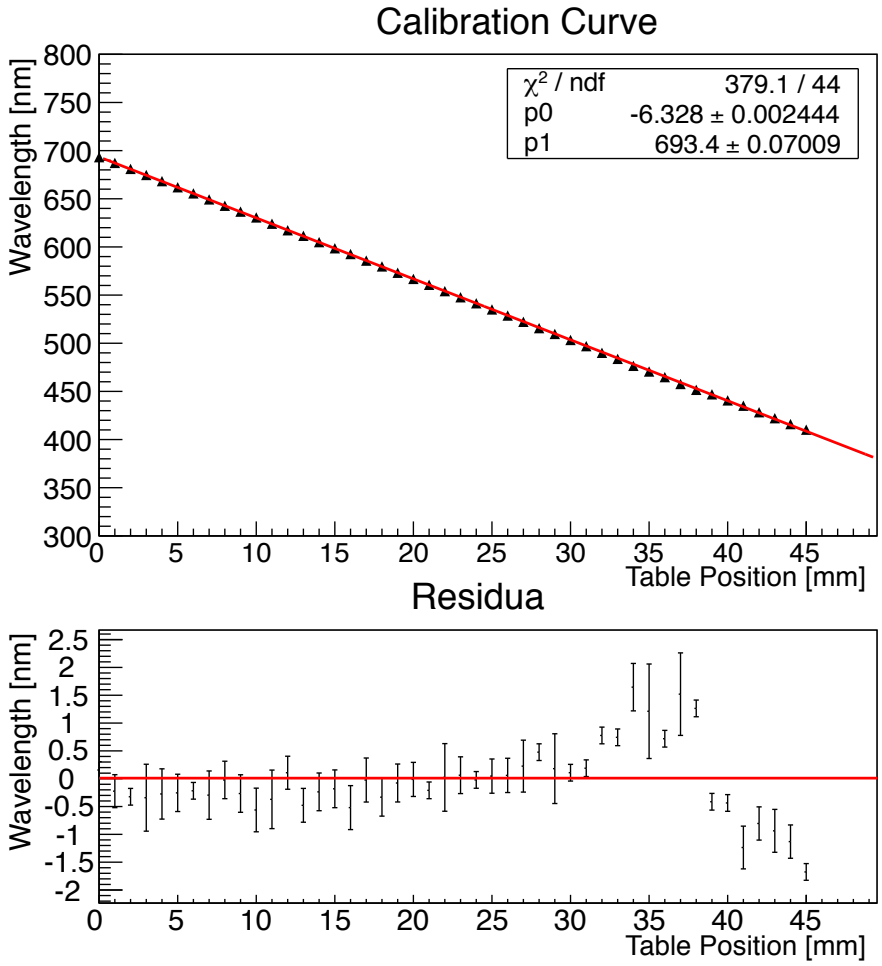

Figure 2.10.: Calibration pickup position to wavelength (above), and the corresponding residua (below).

Keithley Sourcemeter 2400 The sourcemeter is capable of supplying a voltage of 5 µV to 210 V at currents between 50 pA and 1.05 A. The sourcemeter's measurement accuracy consists of 0.015 % of the reading and 1.5 mV basic offset [20]. The sourcemeter is used to supply the SiPM with a bias voltage. For the measurement of the I-V-line in chapter 3.2.1, the readout function is used as well to measure the current through the SiPMs. Communication and data readout are possible via USB connection to the test computer.

Keithley Picoammeter 6485 The picoammeter is a high-accuracy gauge for measuring low currents between 20 fA and 20 mA at a resolution of 10 fA. The specifications for the different measurement ranges can be found in the appendix (cf. Fig. B.16). To reach the manufacturer's specifications, it is important that the

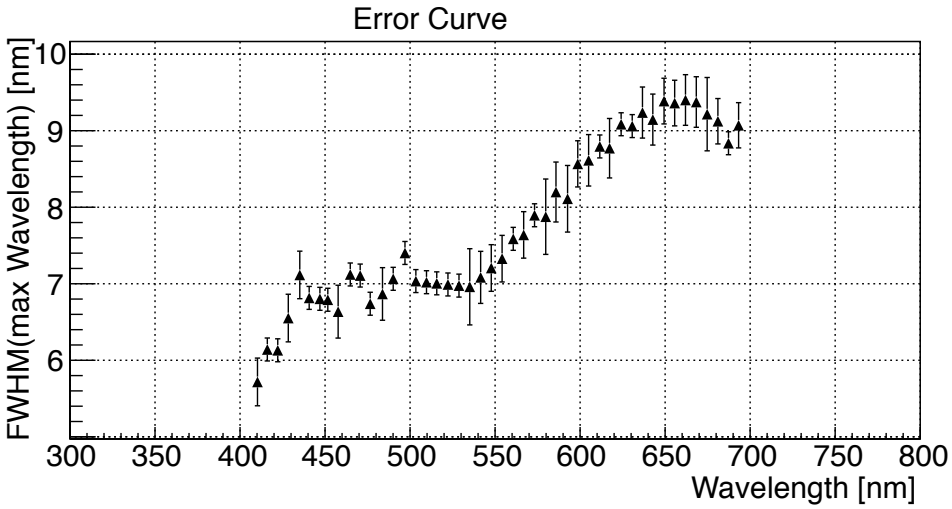

Figure 2.11.: FWHM distribution for the different wavelengths where the light was picked up at.

device is switched on one hour before data taking to function fully stable. The picoammeter is used to read the PIN diode current at different stages. Readings are taken by computer via USB connection. The device has unfortunately proven to be drifting over longterm measurements, hence before and after measurements that included light, dark spectra were recorded to estimate that drift.

Hamamatsu PIN diode S9195 Hamamatsu's PIN diode S9195 is a 5x5 mm calibrated silicon-based photodiode. It can be used in the spectral range of 320 nm-1000 nm to detect light. Its wavelength-dependent photo sensitivity can be found in Fig. B.18. The PIN diode is used as a reference detector for the photon flux and to determine absolute photon numbers. The PIN diode is stabilized through operating it with a 5 V bias voltage.

Wiener VM-USB The VM-USB is a VME master module installed in the CAEN VME64 8100 crate housing several other modules for the characterisation measurements. It is used to communicate with the other programmable modules via USB connection through the test stand's personal computer running the measurement software.

CAEN QDC V965 CAEN's charge-to-digital converter V965 is used in a VME crate and has 16 input channels integrating negative signals and a gate

common to all channels expecting NIM signals. The gate can be either operated with a termination resistance and hence recordings are done all the time, or a signal can be used to generate time windows in which data is taken. In the later case, the gate signal needs to precede the signal to be measured by >15 ns [21]. The signals recorded by each of the QDC's channels is converted by two ADCs in parallel, of which the one in use for the measurements (high range) has a x1 gain stage. The high range's 4096 channels accord to $(0-900)$ fC charges.

CAEN CFD V812 The constant fraction discriminator (CFD) is generally used to create ECL pulses from signals with varying lengths and pulse heights but short rise times. It requires negative pulses, selectable by a threshold value. This threshold can be set between -1 mV to -255 mV in 1 mV steps. This is important for the pre characterisation as will be shown in chapter 3.2. Further settings are the output-pulse width between 15 ns and 250 ns and a dead time, within 150 ns and 250 µs.

CAEN NIM-ECL/ECL-NIM Translator The NIM-ECL/ECL-NIM Translator V538 A translates NIM[6] (high) signals to ECL[7] and the other way around. Since the CFD generates ECL signals, but the QDC requires NIM pulses to be triggered, the signals need to be translated.

Philips Scientific Quad Linear Gate Fan-In/Out 744 The QDC input signals must not exceed 15 mV [21], hence the signals are not fed directly into the QDC but are shifted through a linear fan-in/out and controlled with an oscilloscope so that no signals larger than 15 mV occur. Furthermore, the linear fan-in/out is used to multiply the signals and/or invert these.

LeCroy Wavejet 354 The WaveJet 354 is a four channel oscilloscope with 500 MHz bandwidth. It is used for general monitoring of SiPM-pulse shapes and for the p.e. measurement in chapter 3.2.2, preceding the determination of the breakdown voltage in chapter 3.2. It is read out via ethernet.

SiPM connector board The SiPM connector board is designed at the 3A electronics department[8] and used to invert and preamplify SiPM signals. The cir-

[6] Square-wave pulse with an absolute reference between ground (low) and $-0.6\,\mathrm{V} < V_{\mathrm{pulse}} < -1.6\,\mathrm{V}$.

[7] Square-wave pulse with a differntial signal between $V_{\mathrm{low}} < -1.6$ V and $V_{\mathrm{high}} - 0.6$ V.

[8] Department of 3. Physikalisches Institut A at RWTH Aachen.

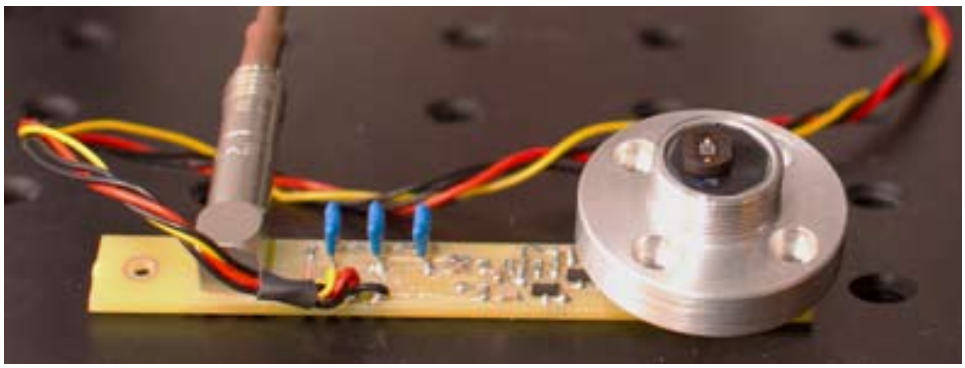

Figure 2.12.: SiPM connector board with SiPM holder and SiPM attached to the holder (Photo: Benjamin Glauß, 2012).

cuit diagram can be found in B.17 and a photograph can be seen in Fig. 2.12. The SiPM is attached to a holder with an external thread (1/2") that can be attached to the integrating sphere. On its back, the holder has two pins the connector board can be attached to regarding correct polarity. The connector board has four connections, two for the SiPM supply voltage, attached to the Keithley Sourcemeter 2400 and two for the integrated preamplifier's[9] supply voltage of 5 V. For noise shielding, the connector board is wrapped in aluminium foil. A LEMO connector is used to tap the preamplified SiPM signal.
When supplying SiPMs with voltage in general, it is important not to have too large resistances in the supply chain. If the photon flux incident on an SiPM changes, the current through the SiPM changes as well. This would result in an unwanted voltage regulation due to a change in the current. For our purposes, a 240 Ω and a 100 Ω resistor were chosen, each one grounded over a 0.1 μF capacitor for filtering purposes.

Philips Scientific Fast Pulse Preamplifier 6954 To further amplify the signals, the already preamplified[10] signals are amplified by a factor five in the Philips amplifier. It is supplied with a Voltage of 12 V.

Tektronix Arbitrary Function Generator 3252 The function generator (AFG) is used to pulse the LEDs on the board described in chapter 2.1.1. It can generate different waveforms such as sine or gaussian pulses with frequen-

[9] Transistor amplifier, using the transistors BFR93A and BFT92 (cf. Fig. B.17), delivering a gain of 50.
[10] The preamplifier that is attached to the SiPM connector board.

cies between 1 mHz and $\sim$100 MHz. Per channel, it can supply a peak-to-peak voltage of 5 V_{pp} with an offset of $\pm$2.5 V. In our case, we use rectangle pulses to flash the LEDs, where the maximum frequency is limited to 120 MHz, that suits our purposes since we use frequencies of the order of $\sim$1 kHz (limited by QDC readout frequency). The AFG is controlled via USB.

3. SiPM Characterisation

3.1. Principle of Measurements

One of the main aims of the setup is to have an easy-to-use process chain with as little user input as possible. For each step in the single measurements, programs are written to record data and analyse the recorded data, eventually calculating the SiPMs characteristics. All these programs are combined in unix shell scripts. For example, one script controls the determination of operating parameters (breakdown voltage, etc.), another one for the relative p.d.e. measurement and so on. Every SiPM is inserted into the setup as a first step and afterwards the scripts are used to take data and characterise this SiPM. The measurements done in this work are the pre-characterisation and the determination of relative and absolute p.d.e. Later, determination of noise phenomena as mentioned in Chapter 1 can be incorporated into the existing setup, adding the necessary routines as programs.

3.2. Pre-Characterisation

The setup and its hardware for the SiPM pre-characterisation is shown in Fig. 3.1. As an example SiPM, the model S10362-100C with 900 pixels by Hamamatsu (cf. Fig. 1.1) is used throughout the measurements. The SiPM is attached to an integrating sphere through a neutral density filter (Chapter 2.1.2, necessary for later measurements) and no light is coupled into the sphere, hence all measurements carried out for pre-characterisation are dark measurements and performed at room temperature. The SiPM's voltage is supplied through a sourcemeter that also reads the current through the SiPM. The inverted (originally positive) and preamplified SiPM signal is led into a second amplifier, shown in Fig. 3.1. After amplifying the signal, it is split into three signals using a linear fan in/out, feeding an inverted and hence again positive signal into an oscilloscope.
Two negative signals are each fed into a CFD and a QDC respectively. The CFD generates ECL signals. These are converted into NIM pulses in an ECL to NIM

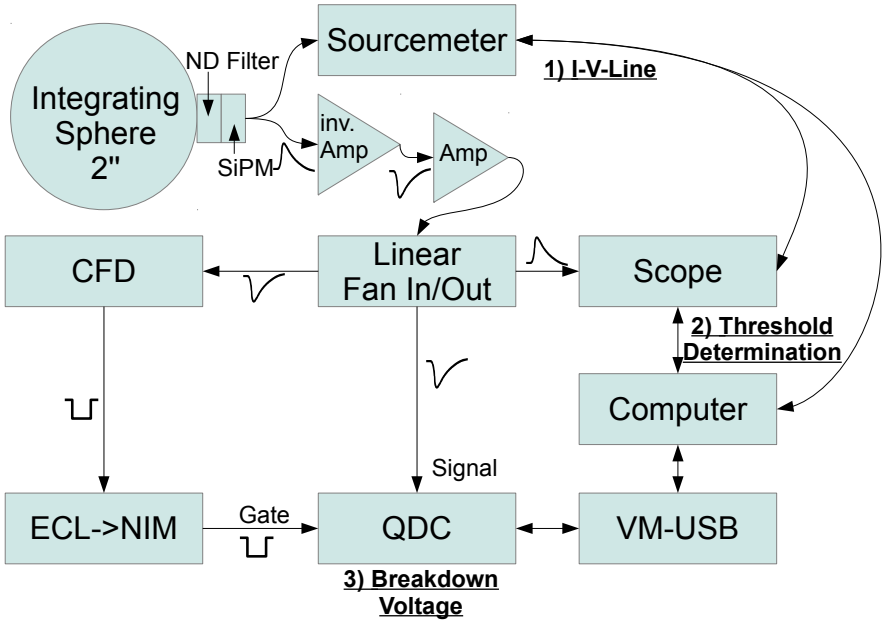

Figure 3.1.: Schematic depiction of the setup for an SiPM pre-characterisation. Note the three consecutive steps for the three measurements included.

converter. The NIM pulses are used to give the QDC a time window for measurements. Choosing adequate cable lengths on both signal ways, one can make sure the gate signal precedes the signal to be integrated by the required 15 ns (cf. Chapter 2.2). Fig. 3.2 shows the gate and the SiPM signal that are fed into the QDC. The yellow gate controls the time span, within which the QDC channel the SiPM signals (pink) is fed to, integrates charges. A gate is always created when the SiPM readout delivers a signal above a certain threshold value to be set in the CFD, but not more often than every 250 ns (CFD dead time). The actual area that is integrated is marked through two white vertical lines, where the first line is shifted by 15 ns regarding to the gate signal's falling edge, and the second line following after another 20 ns, marking the endpoint of charge integration. The whole setup is darkened by a box, in addition to the fact, that the integrating sphere itself is completely closed. The three measurements to be taken in the pre-characterisation are:

In 1), a rough estimator of the scanning region is sought and an approximate value for the breakdown voltage is found. With this approximate information of the SiPMs working region, the SiPM noise frequencies are monitored in step 2) for

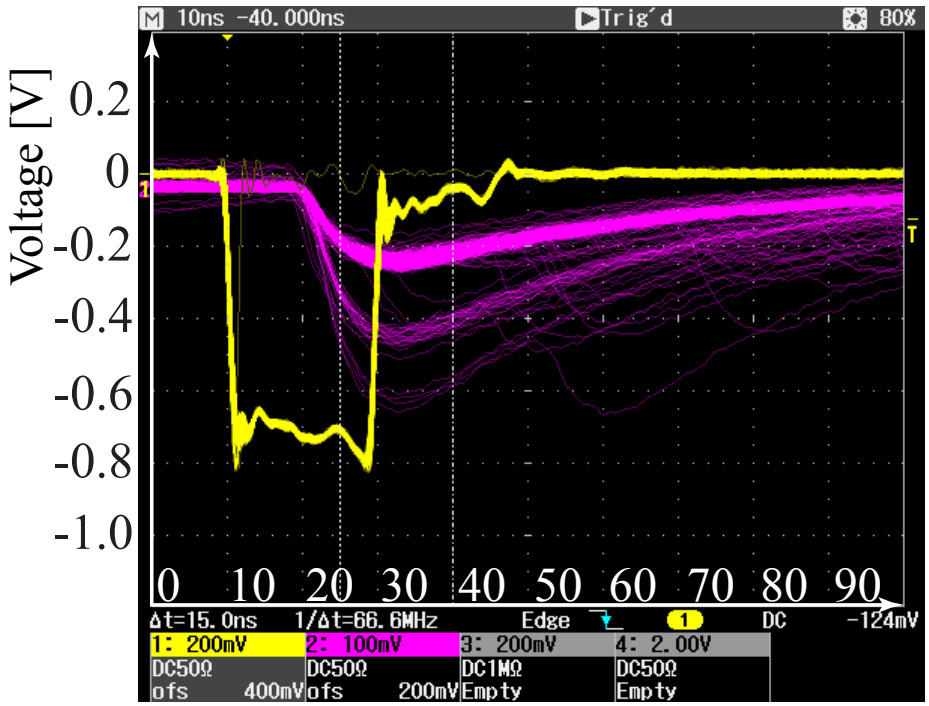

Figure 3.2.: Gate (yellow) preceding the SiPM signal (pink) by 15 ns. The gate triggers the QDC recording, integrating the signals inside of the gate (de facto the vertical white lines).

Pre-Characterisation Measurements

Step #	Measurement	Characteristic	Gauge
1)	I-V-Line	Approximate Breakdown Voltage	Sourcemeter
2)	Threshold Scan	0.5 p.e. Threshold	Oscilloscope
3)	Gain	Breakdown Voltage	QDC

a fixed SiPM current and varying trigger threshold at the oscilloscope. This way, the pulse height for one photon equivalent (1 p.e.) is determined and eventually a threshold can be set at the CFD suppressing signals below 0.5 p.e. that account for noise and generating only gate signals for SiPM signals above this 0.5 p.e. threshold. In step 3) finally QDC dark spectra a recorded, varying the SiPM's supply voltage to determine the absolute gain, since for an increasing V_{OV} and hence V_{bias} as shown in Eq. 1.1 and 1.2. Detailed information about the single measurements can be found below.

3.2.1. I-V-Line

The first step for the pre-characterisation of an SiPM is to gain knowledge about the region within which it operates. This region varies from SiPM to SiPM and

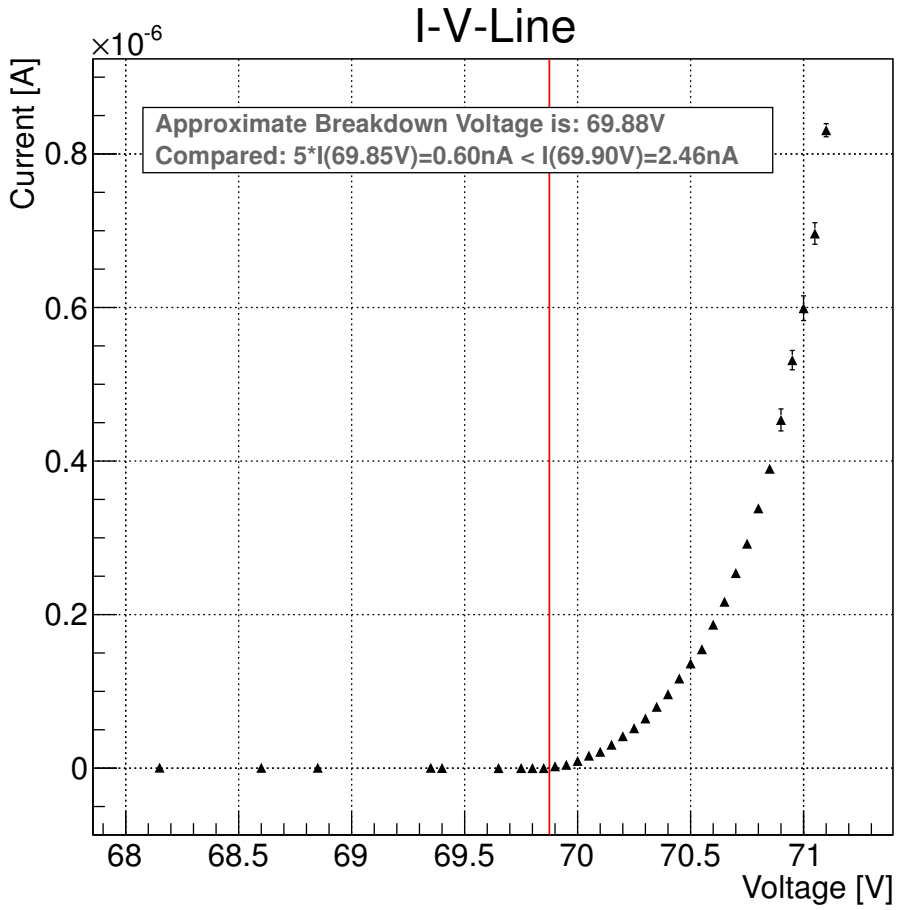

Figure 3.3.: I-V-Line for a Model S10362-100C Hamamatsu SiPM.

can be roughly estimated by the user through evaluation of an SiPM data sheet. In this measurement, on assumes an operating principle similar to the one of a usual diode. The bias voltage is increased until a current can be measured that is significantly higher than the dark current. This voltage is then taken as a first approximation for the SiPM's breakdown voltage, but with a less accuracy than reached later in 3.2.3, rather focussing on a quickly determinable first estimator. In the characterisations carried out, measurements are started roughly 5 V below the operating voltage given by the manufacturer at 70.78 V. The SiPM's bias voltage is increased in steps of 1 V, building an average of three values per step throughout the whole measurement, until a given maximum voltage or a compliance current is reached, the latter is set to 100 µA for safety reasons, since too high currents would damage the SiPM. Whenever one of the limits is reached, the voltage is decreased again in 0.1 V steps until the current underruns 10^{-6} A. The

steplength is decreased again to a value of 0.05 V and measurements are taken and plotted for another 3 V below that point of changing steplength finally. The dataplot (cf. Fig. 3.3) shows the measured value for this 3 V regime. Data evaluation is happening through applying a moving average over five current values, beginning at the low-end side of voltages, comparing each average current value I_n to the current value I_{n+1} recorded at the next higher voltage. For $I_{n+1} > 5 \cdot I_n$, the current increase is considered significant, and a value $(V_n + V_{n+1})/2$ is chosen as an approximate breakdown voltage. In the example shown, the determined value is $V_{\text{BD, approx.}} = (69.9 \pm 0.05)$ V. The current values that were compared are $I_n = 0.12$ nA and $I_{n+1} = 2.46$ nA. The error estimator follows the fact, that the voltage steplength is chosen to be 0.05 V. The accuracy limitations of this measurement are given by the fact that fitting the I-V-line was not possible with reasonable fit functions (i.e. exponential, exponential with polynomial modification as a factor, etc.). Also, the picoammeter's fluctuations in the SiPM's voltage region below V_{BD} do not allow for higher accuracies than determining a breakdown voltage within 0.5 V. The missing datapoints in the plot below $V_{\text{BD, approx.}}$ are due to negative values recorded, erased in the analysis. Hence, only the datapoints used for the analysis are shown. The determined approximate breakdown voltage is passed on as a start value for the determination of the 0.5 p.e. threshold in the next step.

3.2.2. 0.5 P.E. Threshold Determination

The trigger threshold determination begins with scanning for a reasonable SiPM bias voltage by changing V_{bias}, looking for a sufficient noise level to have a distinct difference between the different photon peaks. Throughout the measurement, data is taken by the LeCroy Wavejet 354 oscilloscope and V_{thresh} is set at the oscilloscope as well. Empiric tests have proven, that $f = 400$ kHz are enough events to see at least three steps (cf. Fig. 3.4). The aim is to determine the voltage difference between two photon-equivalent peaks. The underlying principle is, that for a changing trigger threshold voltage V_{thresh} the signal frequency changes, because certain pulses below the threshold are not triggered anymore (cf. Fig 1.7). Changing V_{thresh} in the region between two maxima, the frequency should change only slightly. Increasing $-V_{\text{thresh}}$ passing through a maximum, the frequency should decrease drastically, since the events below the set V_{thresh} do not account for the total measured events anymore. The scan starts determining a reasonable trigger threshold voltage region first by seeking for a maximum frequency

value in steps of $V_{\text{step}} = 20\,\text{mV}$. At every point throughout the whole measurement, an average of 10 frequencies is calculated. When the maximum frequency f_{max} is found, a scan is started determining the region from $V_{\text{thresh}}(f_{\text{max}})$ until $V_{\text{thresh}}(f_{\text{max}}/10.000) = V_{\text{thresh}}(f_{\text{min}})$. Depending on the width of that region, the oscilloscope has to be adjusted.

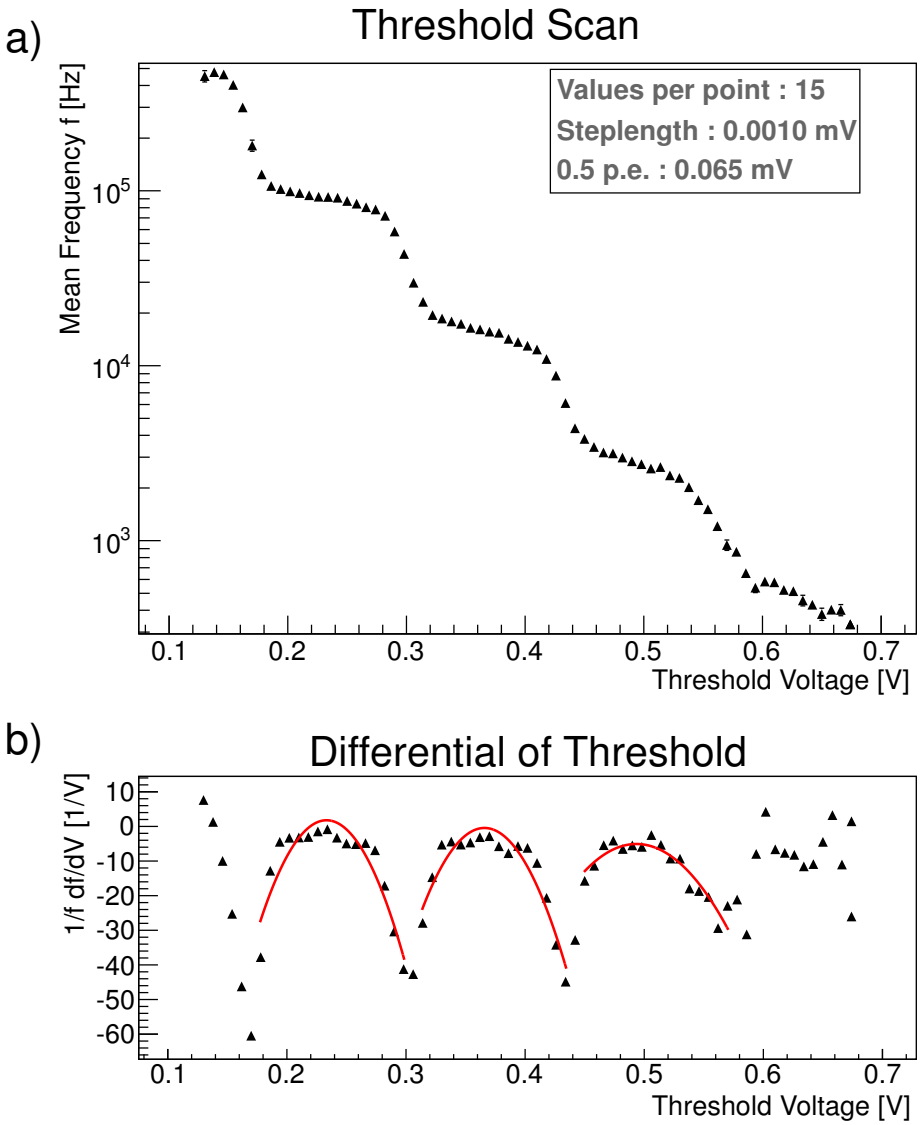

Figure 3.4.: Threshold function for a Model S10362-100C Hamamatsu SiPM. The solid lines in b) are the parabolic fits for determining the 1 p.e. distance.

An adequate voltage step length V_{measure} and voltage resolution $V_{\text{res.}}$ are set, where the former depends on the setting of the latter. Eventually in the example in Fig. 3.4 the actual measurement is carried out between $V_{\text{thresh}}(f_{\text{max}}) = 138\,\text{mV}$ and

$V_{\text{thresh}}(f_{\text{min}}) = 650\,\text{mV}$ in steps of $V_{\text{measure}} = 8\,\text{mV}$. The plotted datapoints give a step-like function where each plateau's width corresponds to a 1 p.e. height. In order to calculate this difference, the numerical derivative is calculated via

$$m_i = \frac{f_{i+1} - f_{i-1}}{(V_{i+1} - V_{i-1})/f_i} \,.$$

The derivative is plotted against the voltage and minima are sought. In the region between these minima, standard polynomials are fitted to the data and the values of the mean positions are extracted. A mean distance between the identified apices is calculated, giving the voltage difference between two photon equivalents depending on the SiPM's supply voltage, returning a value of $V_{\text{thresh}} = 65\,\text{mV}$.
This also means, that one photon equivalent event has a pulse height of 130 mV after passing through the amplifiers. The 0.5 p.e. threshold is set at the CFD, hence only SiPM pulses absolutely higher than V_{thresh} will generate a gate, suppressing signals below this limit. With this setting, electrical noise is filtered.

3.2.3. Breakdown Voltage Determination

The final step for finding an optimal point of operation for an SiPM is the determination of its breakdown voltage. The information gathered above makes it possible to carry out this step in an adequate region of interest for the SiPM to be characterised.
The I-V-Line, as before in the 0.5 p.e. threshold determination gives the region of interest within which measurements are carried out and the 0.5 p.e. threshold suppresses unwanted events. The single steps in this measurement are to record charge spectra with a QDC for different bias voltages of the SiPM, starting with a bias voltage well above breakdown voltage. To make sure the measurement is not taking too long, a timeout limit is integrated, omitting a measurement at a certain bias voltage if no data is recorded within half a second. The supply voltage steps are $\Delta V = 0.05\,\text{V}$. For every spectrum, 750,000 QDC entries are read and written into a histogram, offering a sufficient resolution between the different photon equivalent peaks (cf. Fig. 3.5). For further noise suppression, values below QDC channel number 150 are not taken into account. The different peak positions in the QDC spectrum are due to the different amounts of charge released for different amounts of pixels firing and according to varying pulse heights integrated by the QDC. The higher the signal an SiPM produces the more charge is integrated. Since an optimal SiPM would only have sharp signals, always the same amount

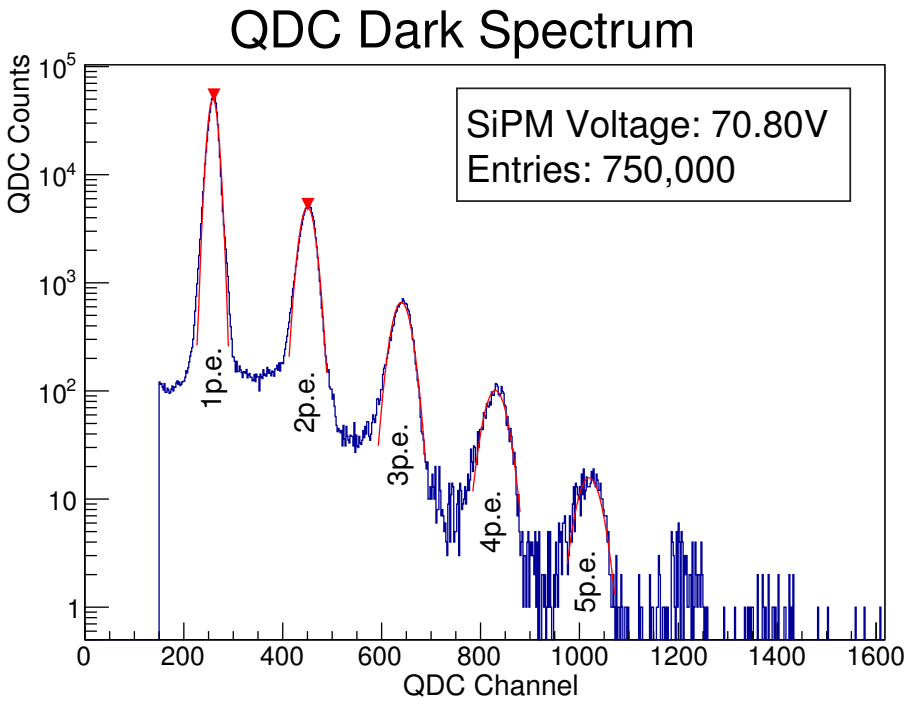

Figure 3.5.: Single QDC spectrum for a Model S10362-100C Hamamatsu SiPM, showing the different photon equivalent peaks.

of charge would be integrated for the same amounts of pixels fired. This number of charge carriers would then be, in case of linearity for low amounts of pixels firing, $n_{\text{pixels}} \cdot G$, where G is the SiPM's gain (cf. Eq. 1.2).
The QDC grades these integrated charges in 4096 channels and the calculation of charge carriers integrated simply is $n_{\text{C}} = QDC_{\text{Channel}} \cdot 0.2\,\text{fC}$. For the same amount of pixels fired, signals accumulate in one channel and the peaks take shape. When changing the SiPM's supply voltage, the peak distance changes (i.e. it increases with increasing bias voltage), giving a mean to determine the SiPM's absolute gain and furthermore its breakdown voltage. The dependency of the peak distance Δ_{p} on the over voltage V_{OV} is linear. Hence the over voltage

$$V_{\text{OV}} \sim d_{\text{peak}} \tag{3.1}$$

and thus d_{peak} is equal to zero for a vanishing over voltage. For the used SiPM nine QDC spectra (cf. Fig. 3.5) at different voltages are evaluated, even though more are recorded but sorted out due to stability criteria to guarantee a robust value. For too low over voltages, the evaluation of the peaks is not sufficient, so only those spectra where at least four peaks could be identified reliably are

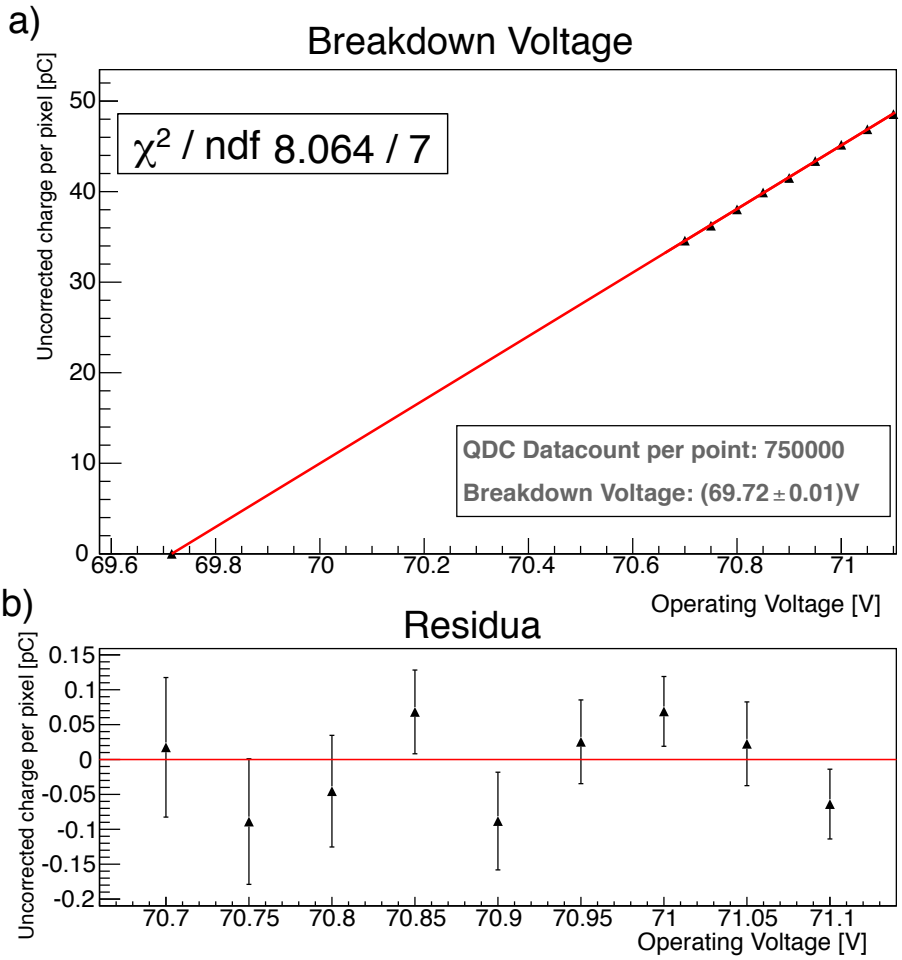

Figure 3.6.: Threshold function for a Model S10362-100C Hamamatsu SiPM.

chosen for the breakdown voltage analysis. If more peaks are found, nevertheless only four are used for reasons of consistency. The peak analysis is carried out by finding the first two peaks in a spectrum (positions p_1, p_2) through the built-in peak finder *Search()*[1] in the ROOT framework[2]. The distance $p_2 - p_1 = d_{\text{peak}}$ between these is calculated. Subsequently every peak n in the spectrum at positions $p_n = n \cdot d_{\text{peak}} + p_1$ $(n = 0, ..., 3)$ is fitted twice with a gaussian distribution. The first fit will give an approximate position and width of the peak and the second fit will be carried out around the the determined center within a 1.5σ region. Eventually, out of each of the nine evaluated spectra an uncorrected charge per pixel in units of pC could be extracted to the related over voltage. The values are shown in Fig. 3.6, where a linear function was fitted to. It gives a break-

[1] Of the TSpectrum class
[2] http://root.cern.ch/

down voltage of $V_{BD} = (69.72 \pm 0.01)$ V. The manufacturer does not provide a breakdown voltage for its products, but an operating voltage, higher than the breakdown voltage. In this case for the used SiPM, the given operating voltage is $V_{OP} = 70.72$ V. The breakdown voltage that is determined through the relative gain in this case of $V_{BD} = (69.72 \pm 0.01)$ V is compared to the value of the approximate breakdown voltage $V_{BD,\,approx.} = 69.9 \pm 0.05$, determined using the I-V-line, compatible within a 4σ region. Nevertheless, as mentioned in Chapter 1, the breakdown voltage is temperature dependent. It can shift with a factor of $\beta = 56\,\mathrm{mV/K}$ (cf. [1], [10]). Hence, a possible temperature shift of about 3 K between the measurements can explain this discrepancy.

3.2.4. Photon Equivalent Peak Width

In the next measurement, the width of the photon equivalent peaks for a different number of firing pixels of an SiPM in a QDC spectrum is analysed. The peaks' behaviour change with the according amount of firing pixels, i.e. the more pixels fire, the more the peak width increases. This can be used as a measure of pixel uniformity, since the width of the 1 p.e. peak represents the statistical dispersion of the different pixel capacitances.

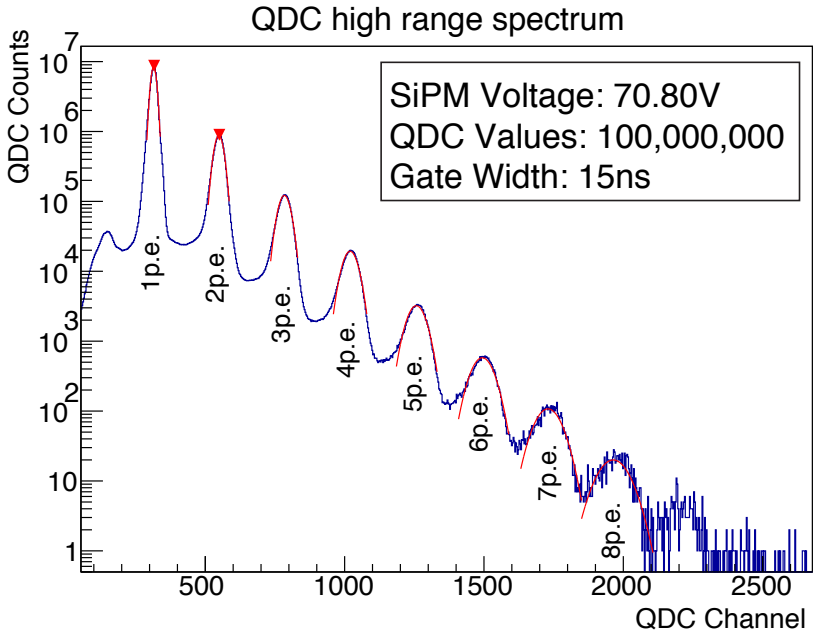

Figure 3.7.: High statistics QDC spectrum for a Model S10362-100C Hamamatsu SiPM.

A further spectrum is recorded at a bias voltage of $V_{\text{bias}} = 70.72$ V. In this case, within one hour 100,000,000 events are recorded with the same setup as above. As a gate width, 15 ns are chosen. Due to the large amount of data, up to eight photon equivalent peaks are clearly distinguishable from each other (cf. Fig. 3.7). The fits are carried out in the same manner as for the determination of the breakdown voltage, but more peaks are taken into account. The limit for a fit's width is set to 100 channels. Is a peak's width larger than these 100 channels, it is not taken into account anymore. Eight peaks suit this limitation.

Table 3.1.: Photon Equivalent Peak Characteristics for 1.5σ integration width

Peak #	QDC Position [pC]	Width [pC]
1	62.99 ± 0.01	2.11 ± 0.01
2	109.82 ± 0.01	3.49 ± 0.01
3	156.86 ± 0.01	4.60 ± 0.01
4	204.17 ± 0.01	5.73 ± 0.01
5	251.81 ± 0.03	6.89 ± 0.04
6	299.33 ± 0.08	8.15 ± 0.09
7	346.72 ± 0.19	9.12 ± 0.19
8	393.72 ± 0.47	10.5 ± 0.46

As mentioned before, the peaks represent a certain amount of firing pixels. The increasing width of peaks is due to the combination of the pixels' statistical dispersion. Every pixel has a capacitance that might slightly differ from the rest, and hence not always the exact same amount of charge carriers is produced in an avalanche for different pixels. Table 3.1 gives the values characterising the peaks in Fig. 3.7. The peaks' width versus position are shown in Fig. 3.8. The black markers in Fig. 3.8 correspond to values one gets, setting an integration width of 1.5σ around the center value. The green and blue markers show the deviations for changing the integration width, resulting in a systematic over- or underestimation. The factors giving the ratio $(n+1)$p.e.$/(n)$p.e. between the width of peak $(n+1)$ an the preceding peak width of peak n are evaluated. Building a weighted mean gives an increase in width of 1.479 ± 0.001. This value makes sense, since each pixel's capacitance when statistically combined leads to quadratically added uncertainties. Hence, the widths are quadratically added, too. This would ideally lead to a factor of $r = \sqrt{2}$ for $r = (n+1)$p.e.$/(n)$p.e. The difference to $\sqrt{2}$ can be explained with a deviation from this prediction due to a shift in the signals' baseline, increasing each width. In this analysis, it becomes obvious, that a further understanding of the background would be necessary for more reliable peak

position parameters. A change of the fit's width would cause these positions to prove being rather unstable. But for a suitable choice of a fit region (in this case 1.5σ), the ratio width/peak distance is constant. The plot shown in Fig. 3.8 shows the deviation for a choice of certain different fit regions. The error on the peak width is due to the peak fit in Fig. 3.7.

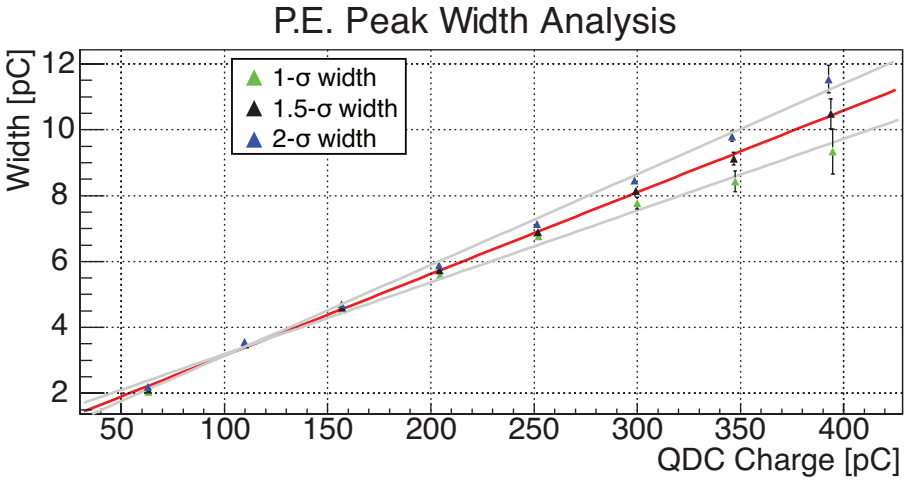

Figure 3.8.: Peak width analysis for peaks in Fig. 3.7, using different fit widths. The red line shows the fit for 1.5σ, the grey lines for 1σ and 2σ respectively.

3.3. Photon Detection Efficiency

The final step of SiPM characterisation in this thesis is the determination of an SiPM's photon detection efficiency. The p.d.e. is a measure for an SiPM's probability of detecting photons. It is the ratio between photons detected by the SiPM to the amount of photons actually incident to the SiPM. The p.d.e. depends on several quantities as shown in Eq. 1.3, that are the quantum efficiency $Q.E.$, the Geiger probability for creating an avalanche breakdown and the geometrical factor showing the ratio between active to its total area. As mentioned before, the measurements of relative and absolute p.d.e. differ in setup and data analysis, as will be further explained. The relative p.d.e. per wavelength only tells whether more or less photons are detected at a certain wavelength compared to another. The absolute scale is gained through absolute p.d.e. measurements, where the number of photons is counted, and data is only taken within a narrow time frame in case that the pulsed light source is active. Both measurements are eventu-

ally combined, scaling the relative data to the absolute p.d.e. numbers, giving an SiPM's photon detection efficiency over the white LED's whole regime.

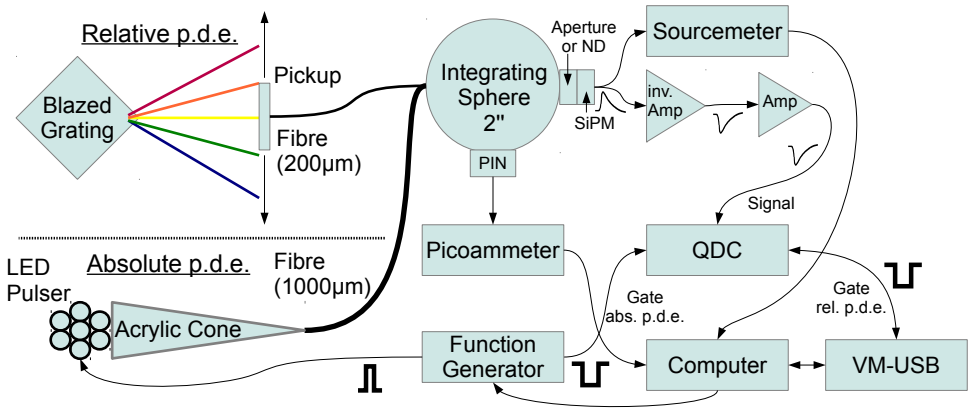

Figure 3.9.: Setup for p.d.e. measurements. For relative p.d.e. determination, the upper light source is used (white LED, fanned out spectrum through grating, movable light pickup for picking up different wavelengths), absolute measurements with the light source below(pulsed LEDs).

The setup for the p.d.e. measurements needs to be slightly altered compared to the one used for the pre-characterisation, including the light sources to be exchanged when switching from relative p.d.e. (constant flux, white LED) measurement to the one for an absolute p.d.e. (monochrome, pulsed LEDs). The setup is depicted in Fig. 3.9. All measurements are carried out at room temperature. For a clear appearance, parts of the optic table preceding the grating are omitted, please refer to Chapter 2.1 for the complete optical setup. Following changes in this differ from the one used in the pre-characterisation chapter: Linear fan in/out, CFD and NIM->ECL converter are not necessary anymore since the gate is given by the function generator that also pulses the LEDs. The amplified SiPM signal is now fed directly into the QDC. For absolute p.d.e. measurements, the ND filter is exchanged for a 0.5 mm diameter pinhole, opened in such way, that only a certain area of the SiPM is illuminated. Afterwards, a ratio can be calculated between the light yield at the openings used for the PIN diode and the SiPM (cf. chapter 3.3.2).

3.3.1. Relative Photon Detection Efficiency

For measurements of relative SiPM p.d.e., the gauges read are the pico ammeter reading currents from the PIN diode on the one hand, and on the other the source meter, reading the SiPM's current. As light source, the fanned out white LED's light is picked up at the movable pickup and coupled into the integrating sphere. The basic principle used is, that the current flowing through the SiPM is proportional to the amount of photons incident on the SiPM's surface [9]. The PIN current is measured simultaneously to correct the SiPM signal relatively for the photon flux. For every current measured at either the PIN oder the SiPM, a shutter can be closed, and no light will enter the integrating sphere for dark measurement reasons. This shutter is attached to the tube, holding the collimator lenses, between lens two and the blazed grating, i.e. no light is incident on the grating. To take data over the whole available spectrum, the light pickup is moved in steps of 1 mm and all four measurements mentioned are carried out at each step. To calculate the wavelengths at each point where data is taken, the calibration results from Chapter 2.1.3, shown in Fig. 2.10 are used. The first step of data analysis is the same for the SiPM and the PIN current, since both sets of currents $I_{\mathrm{SiPM,raw},\lambda}$ and $I_{\mathrm{PIN,raw},\lambda}$ (cf. Fig. 3.10a) and 3.11a)) at each given wavelength λ are corrected for the dark values $I_{\mathrm{SiPM,dark},\lambda}$ and $I_{\mathrm{PIN,dark},\lambda}$ (cf. Fig. 3.10b) and 3.11b)). In the latter plots, one can see a systematic drift of the background values for both measurements, that can be traced back to a change in temperature. A rising temperature would cause the PIN's dark current to rise due to more charge carriers produced because of thermal excitation. An SiPM's dark current on the other hand decreases for higher temperatures as the breakdown voltage rises, but the over voltage is set to a constant value (see Eq. 1). Hence, the signal depending on the bias voltage falls (cf. Eq. 1.1). The effect is minimised by measuring illumination values and dark values one after another before moving the pickup to the next position. The results of the background correction in $I_{\mathrm{SiPM,corr},\lambda}$ and $I_{\mathrm{PIN,corr},\lambda}$ is shown in Fig. 3.10c) and 3.11c). Comparing the recorded data to the white LED's spectrum in Fig. 2.3, one can recognize the LED's characteristic behaviour. Since the PIN diode is not uniform in detection efficiency throughout the visible spectrum, it needs to be corrected for calibration values given in a data sheet (see Appendix B.18). The wavelength-dependent absolute photon count per time and unit area can then be calculated via

$$N_{\gamma,\lambda} = \frac{I_{\mathrm{PIN,corr},\lambda}}{QE_{\lambda} \cdot e \cdot a} \,,$$

where e is the elementary charge, $a = 25$ mm^2 is the PIN's surface area and Q.E. the PIN diode's wavelength dependent quantum efficiency. The calculations' outcome per datapoint is shown in Fig. 3.10d). As the last but one step, the SiPM's corrected current values $I_{\mathrm{SiPM,c,\lambda}}$ in Fig. 3.11c) are divided by the photon numbers $N_{\gamma,\lambda}$ in Fig. 3.10d). This results in the SiPM sensitivity values plotted against the wavelength in Fig. 3.11d).

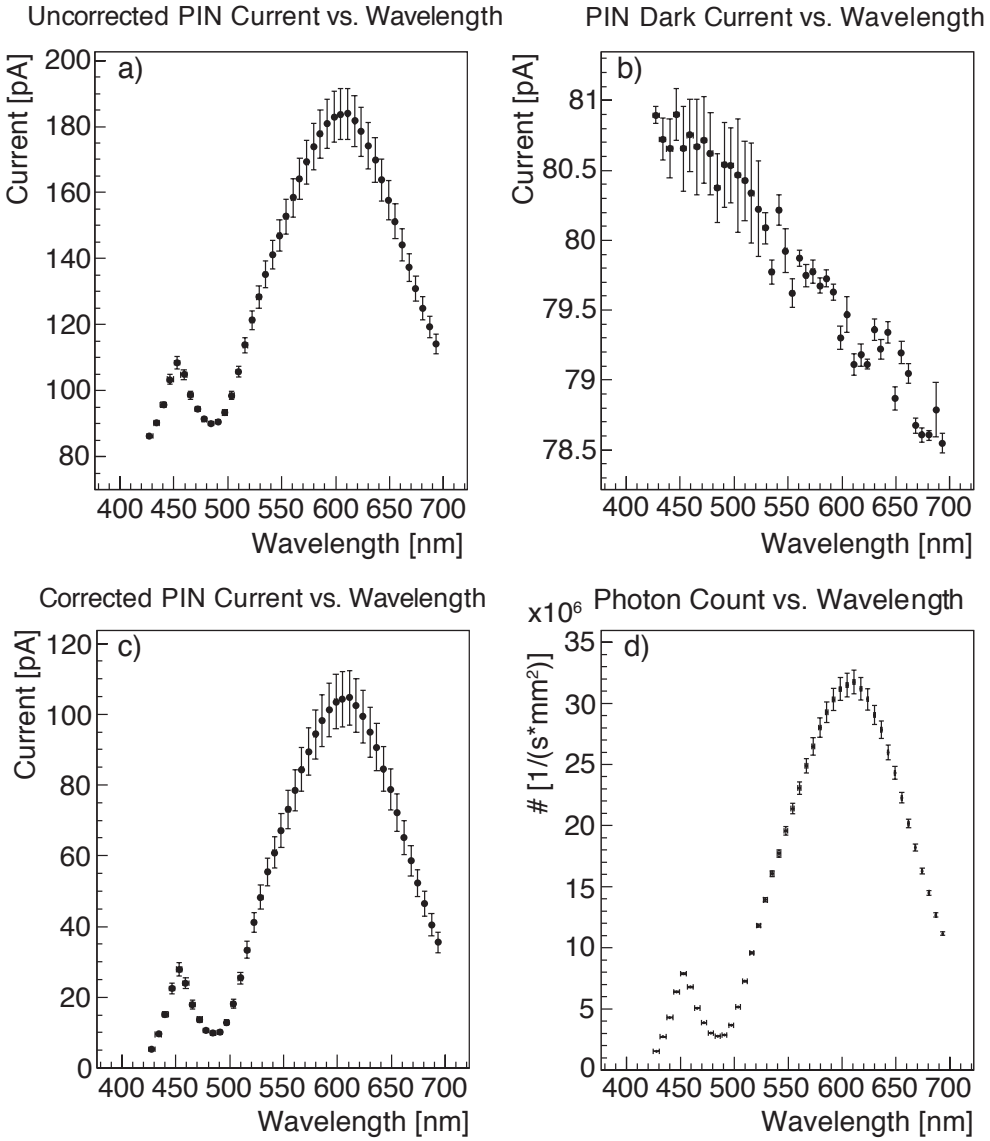

Figure 3.10.: Evaluation of PIN diode currents behind the integrating sphere, measured with a picoammeter. a) shows the raw current, b) shows the dark current, c) shows the difference between the values in a) and b), d) shows the photon count, incorporating the PIN diode's sensitivity.

This however is not yet the final relative SiPM p.d.e., since the values still have to be corrected for the ND filter that is attached between the integrating sphere and the SiPM. As shown in Fig. 2.8, this filter's effect is not constant.

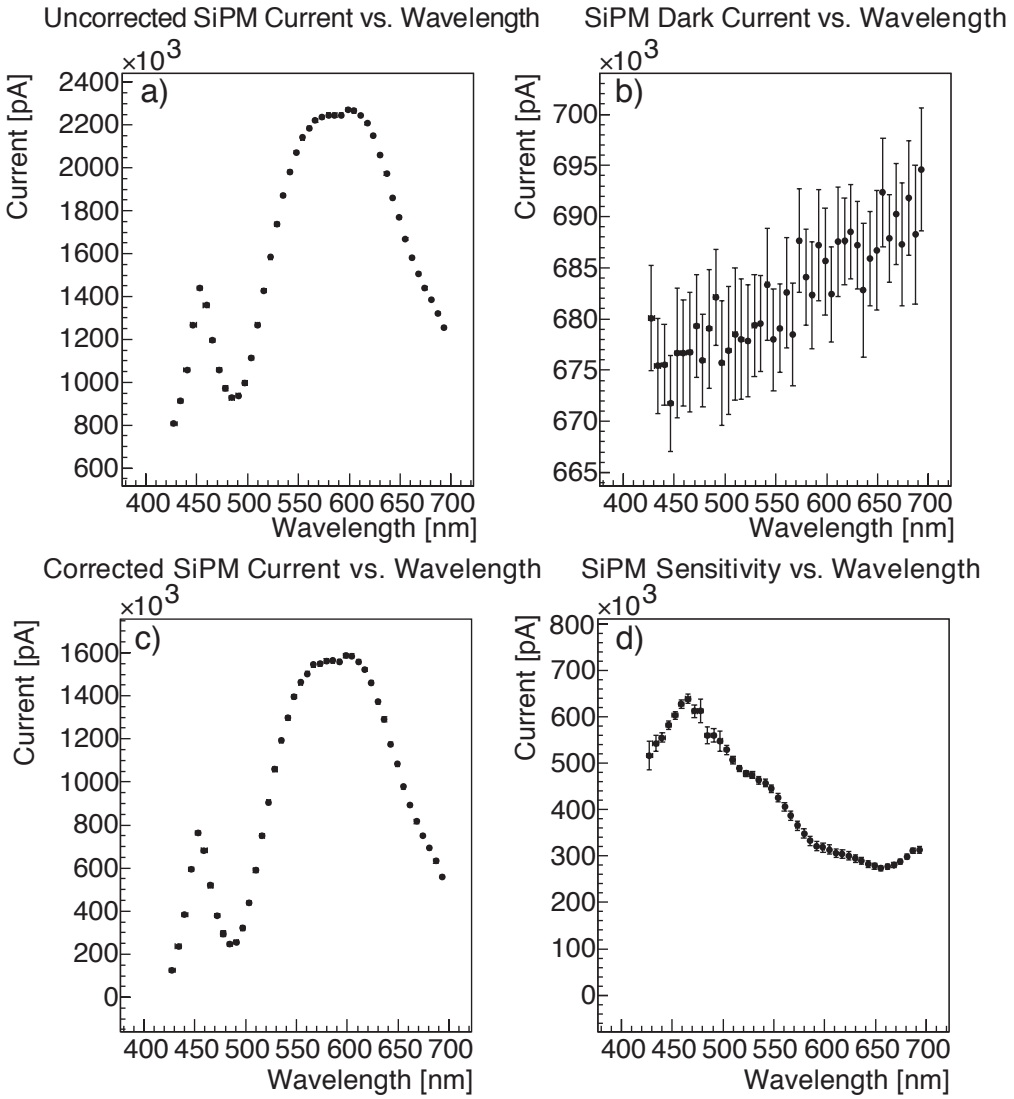

Figure 3.11.: Evaluation of SiPM currents behind the integrating sphere, measured with a sourcemeter. a) shows the raw current, b) shows the dark current, c) shows the difference between the values in a) and b), d) shows the sensitivity data from c) divided by that from 3.10c), not corrected for the ND filter.

The calculated values for this filter's ratio are multiplied with the SiPM's sensitivity and the largest value is normalized to unity, giving the relative p.d.e. in Fig. 3.12. The curves qualitative trend does match the characteristics of the p.d.e. given by the manufacturer in Fig. 1.8 for a related model, but it has neverthe-

less a wide plateau and maximum values are in a higher wavelength region than compared to the manufacturer's plot.

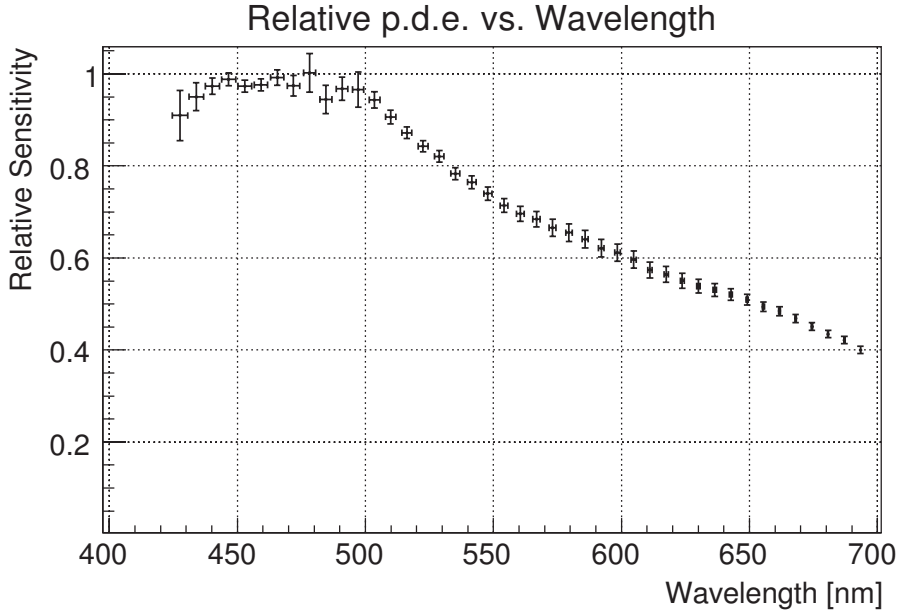

Figure 3.12.: P.D.E. values for a Model S10362-100C Hamamatsu SiPM, showing its relative behaviour in the visible spectrum.

3.3.2. Absolute Photon Detection Efficiency

The determination of the absolute p.d.e. requires another change of the setup. The ND filter used before is exchanged for a pinhole with diameter 0.5 mm, mounted between integrating sphere and SiPM in a way that only a fraction of the SiPM's detection area (pixels plus dead space between the pixels) is hit by photons. The data taking is carried out with the QDC again, since it is necessary to record charge distribution spectra. As one can see in the lower left of Fig. 3.9, the gate for this measurement is generated by a function generator, that also pulses the LEDs. Through adjustment of cable lengths and the right choice of the delay between the generated gate signal and the signal used for pulsing the LED, the gate is set similarly to the one in Fig. 3.2 but on the rising SiPM signal edge. This discriminiates the noise on the signals falling edge, that is due to the electric signals coupled into the SiPM signal because of the pulsed LEDs. The LED pulses in this setup can not completely shielded and so the SiPM signals are influenced by that noise. The gate width is empirically set to 12 ns. The LED pulses are $\sim$ 10 ns per pulse, hence only small amounts of photons reach the

SiPM per pulse.
For gaining knowledge about an absolute p.d.e., a reference value is needed, that is measured with a PIN diode. This reference value is equal to the photon number per pulse, that can be calculated through

$$n_{\gamma,\lambda} = \frac{\Delta I_{\mathrm{PIN},\lambda}}{QE_\lambda \cdot e \cdot r_\lambda \cdot f_\mathrm{p}} \ , \tag{3.2}$$

for the LEDs' different wavelengths. The current values $\Delta I_{\mathrm{PIN},\lambda}$ are the difference between $I^{\mathrm{light}}_{\mathrm{PIN},\lambda} - I^{\mathrm{dark}}_{\mathrm{PIN},\lambda}$, measured with the PIN diode while the QDC spectra are recorded with and without pulsed light respectively. Also in the equation, there are the elementary charge e and the pulser frequency f_p of the function generator. The wavelength dependent quantum efficiency of the PIN diode *(QE)* has a relative error of 5 %, given by the manufacturer. The factor r is the ratio for the different positions of SiPM and PIN diode at the integrating sphere. It is calculated by measuring the PIN current for each wavelength on the one hand ${I_\mathrm{PIN}}^{\text{PIN pos.}}$ at the PIN diode's position. There, the PIN diode is used for the later measurements. On the other hand ${I_\mathrm{PIN}}^{\text{SiPM pos.}}$ is measured by mounting the PIN diode behind the pinhole where the SiPM is usually mounted. The pinhole leads to a decreased photon flux, resulting in ${I_\mathrm{PIN}}^{\text{SiPM pos.}} < {I_\mathrm{PIN}}^{\text{PIN pos.}}$. Furthermore, both the PIN diode and the SiPM are installed at a distance of 1 cm away from the integrating sphere to minimise effects to to divergence. Both currents are dark-current corrected. This gives the ratio due to the pinhole and the different positions at each wavelength

$$r_\lambda = \frac{{I_\mathrm{PIN}}^{\text{PIN pos.}}}{{I_\mathrm{PIN}}^{\text{SiPM pos.}}} \ . \tag{3.3}$$

The pulser frequency f_p is set to 100 kHz for recording QDC spectra, even though the QDC readout is limited to 10 kHz[3]. The factor 10 is necessary to make sure that enough light reaches the PIN diode to measure the current differences $\Delta I_{\mathrm{PIN},\lambda}$ needed for calculating the photon count per pulse via Eq. 3.2. The results of $n_{\gamma,\lambda}$ for each wavelength can be found in Tab. 3.2.
With changing the LED's parameters such as voltage and pulse width, the amount of photons per pulse can be controlled, and the setup is adjusted to only have a few photons per pulse. This assures a low event rate to adept to a Poissonian fundament for the analysis ([9], [10]). The statistical errors are given because of multiple measurements with the picoammeter and building a mean.

[3]Nevertheless, it has proven, the QDC tolerates higher gate frequencies, delivering reliable data.

Table 3.2.: Values for the calculation of $n_{\gamma,\lambda}$ through Eq. 3.2.

Wavelength λ	$\Delta I_{\mathrm{PIN},\lambda}[\cdot 10^{-12}\,\mathrm{A}]$	QE_{λ}^{PIN}	r_{λ}	$n_{\gamma,\lambda}$
407 nm	11.4 ± 0.1	0.830	150.6 ± 8.6	5.7 ± 0.3
470 nm	4.5 ± 0.1	0.885	142.3 ± 5.6	2.1 ± 0.1
505 nm	10.5 ± 0.1	0.864	161.2 ± 15.9	4.7 ± 0.4

As already mentioned, QDC spectra for each wavelength are recorded simultaneously while measuring the PIN currents, and a dark spectrum is recorded as well for correction of optical crosstalk and after-pulsing. Through these spectra, the mean number of fired cells $\mu = \mu_{\mathrm{light}} - \mu_{\mathrm{dark}}$ can be calculated. Since one can assume that due to only a few events taking place per pulse (cf. Fig. 1.7, <10 pixels firing at a time), these events follow a Poissonian distribution, and hence

$$p(k) = \frac{\mu^k \cdot e^{-\mu}}{k!}$$

applies. The probability that no photon hits the SiPM is given by

$$p(0) = \frac{\mu^0 \cdot e^{-\mu}}{0!} = e^{-\mu} \ .$$

This probability is equal to the number of events in a spectrum's pedestal (N_{ped}) divided by the total number of recorded events (N_{tot}), resulting in

$$\begin{aligned} p(0) &= \frac{N_{\mathrm{ped}}}{N_{\mathrm{tot}}} \ , \\ \Rightarrow \mu &= -\ln \frac{N_{\mathrm{ped}}}{N_{\mathrm{tot}}} \ . \end{aligned} \tag{3.4}$$

And the error on the mean for a Poissonian distribution can be calculated via

$$\sigma_{\mu} = \frac{\sqrt{\mu}}{\sqrt{N}} \ ,$$

given the respective number of events, N.
This mean number can be calculated for the spectra where the LED is pulsed and for the case where no light is coupled into the integrating sphere respectively to correct for the background. Eventually, this results in

$$\mu_{\mathrm{corr}} = \mu_{\mathrm{light}} - \mu_{\mathrm{dark}} \ . \tag{3.5}$$

The absolute p.d.e. can be calculated with

$$p.d.e._{\text{abs.}} = \frac{\mu_{\text{corr}}}{n_{\gamma,\lambda}} \,. \tag{3.6}$$

The error values for Eq. 3.3, 3.5 and 3.6 are calculated via Gaussian error propagation.

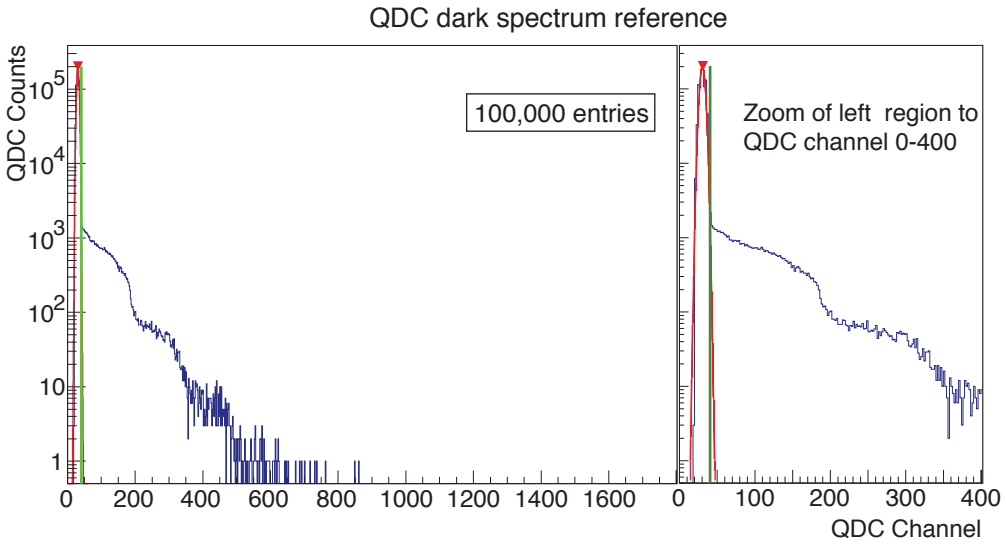

Figure 3.13.: QDC dark reference spectrum, no light coupled into the integrating sphere.

The QDC spectra analysed for getting the numbers N_{ped} and N_{tot} in Fig. 3.4 are shown in Fig. 3.14 through 3.16, and the dark spectrum in Fig. 3.13. The first peak in each spectrum is the pedestal peak, that is due to the setup's intrinsic noise. The spectra before did not show a distinct pedestal, because the gate was always synchronised with events where pixels fire. The pedestal represents the events, where no pixels fired. A Gaussian is fitted around its center position that is found through the ROOT peak finder routine. A limit (green line in Fig. 3.13 through 3.16) is set three sigma to the right of the fit's center position. All entries below that limit are considered to be the pedestal events N_{ped}.
The plots result in the number of fired cells for and illuminated SiPM at the three given wavelengths and for the dark measurement. The results are given in Tab. 3.3.

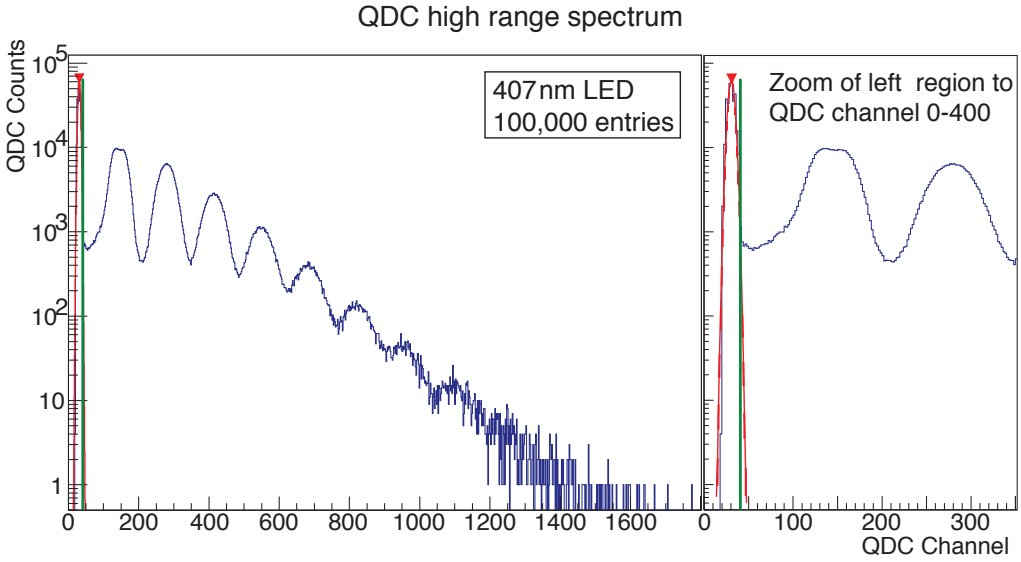

Figure 3.14.: QDC spectrum for a pulsed LED with 407 nm

Table 3.3.: Values for the calculation of $n_{\gamma,\lambda}$ through 3.2.

Wavelength λ	μ_{dark}	μ_{light}	μ_{corr}
407 nm	0.129 ± 0.001	1.127 ± 0.004	1.083 ± 0.004
470 nm	0.111 ± 0.001	0.614 ± 0.003	0.503 ± 0.003
505 nm	0.203 ± 0.002	1.031 ± 0.003	0.828 ± 0.004

At this point, everything needed for the calculation of absolute p.d.e. values is given, and can be carried out using Eq. 3.6, resulting in the values shown in Tab. 3.4.

Table 3.4.: Values for the calculation of the absolute p.d.e.

Wavelength λ	μ_{corr}	$n_{\gamma,\lambda}$	$p.d.e._{\text{abs.}}$
$407\,\text{nm} \pm 5.7$	1.083 ± 0.004	5.7 ± 0.3	$(19.7 \pm 1.0)\%$
$470\,\text{nm} \pm 12.3$	0.503 ± 0.003	2.1 ± 0.1	$(23.9 \pm 1.1)\%$
$505\,\text{nm} \pm 15.5$	0.828 ± 0.004	4.7 ± 0.4	$(17.6 \pm 1.5)\%$

With these values, the results for the relative p.d.e. shown in Fig. 3.12 can be rescaled. The absolute values seem to be underestimated, compared to the results in [9] and [10] for the SiPM that was used. In the work mentioned, the SiPM in use has a peak p.d.e. of about 30 % at an overvoltage of 1 V. Different reasons can explain the underestimation of the p.d.e. values. One can assume, that the corrections carried out for the r_λ values lead to an underestimation of incident

photons, even though pinholes were used to minimise these. Another influence might be the noise due to the short light pulses at voltages of 5 V. This might lead to a shift of entries from the 1 p.e. to the pedestal, underestimating the number of firing cells due to photons.

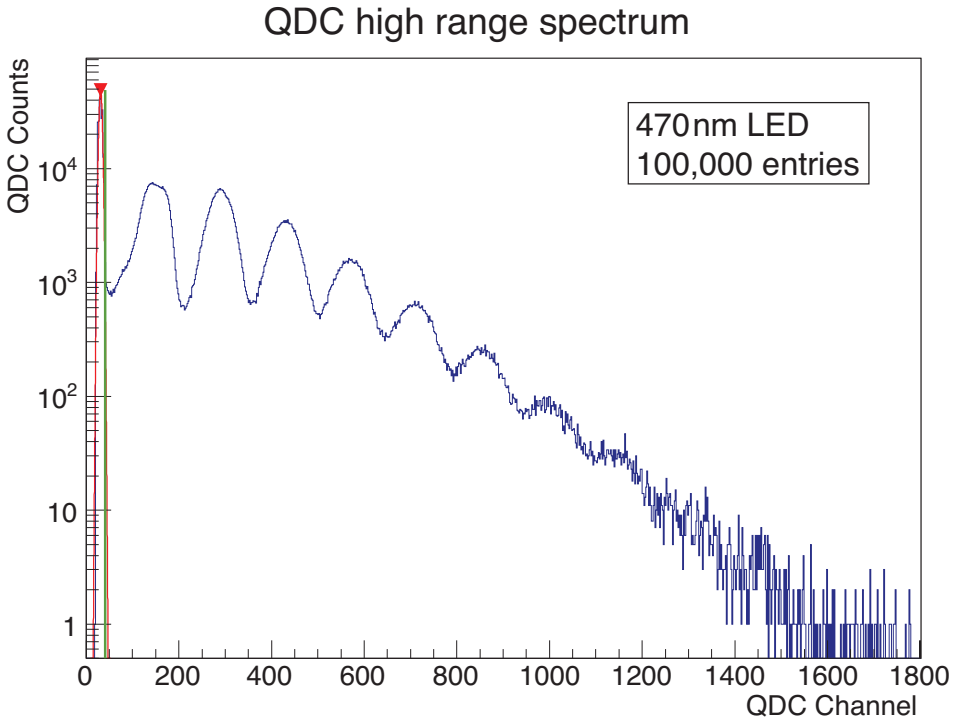

Figure 3.15.: QDC spectrum for a pulsed LED with 470 nm.

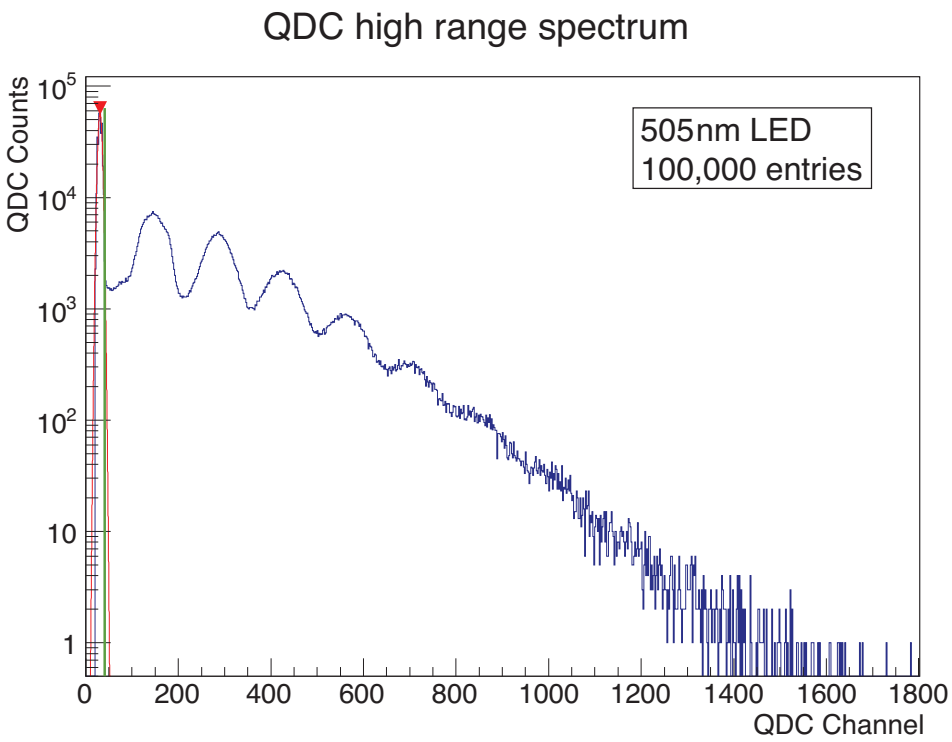

Figure 3.16.: QDC spectrum for a pulsed LED with 505 nm.

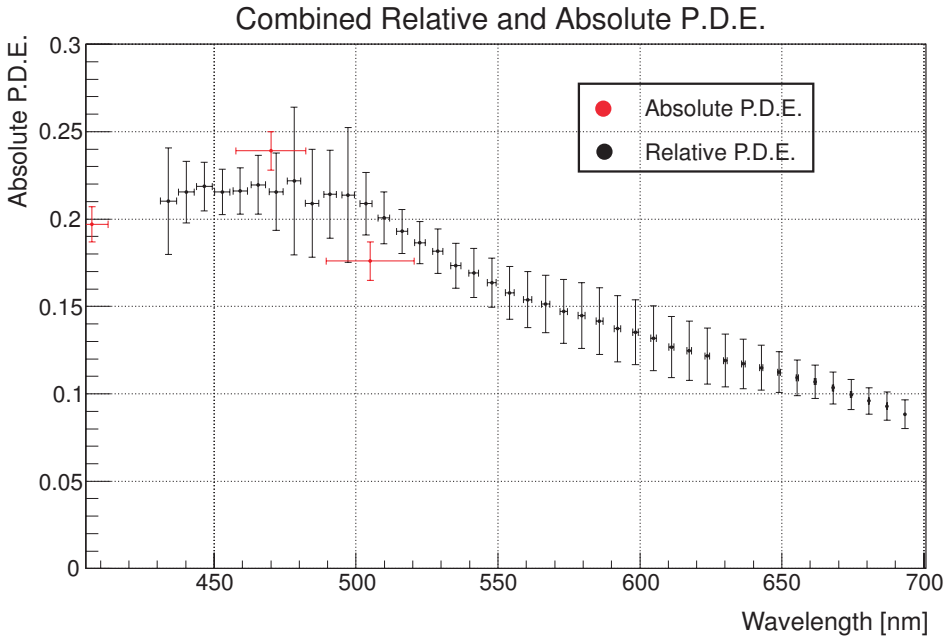

Figure 3.17.: Combined results for the absolute and relative p.d.e. values at an over voltage of 79.72 V for a 100 pixel SiPM, Model S10362-100C.

4. Summary and Conclusion

The aim of this work was to build a test stand that is capable of SiPM characterisation studies at a broad wavelength regime. A further demand was, that everything should work with as little user input as possible and fully automised. This included the determination of the breakdown voltage, the gain determination, noise measurements and finally the relative and absolute p.d.e.
Some tests require different setups, that makes changes in the setup necessary, but these were kept at a minimum degree. The automisation is realised through controlling the hardware completely through shell scripts as well as the data analysis. The analysis is carried out along the measurements and the results are passed on to the next step for measurements depending on the recently gained values (pre-characterisation chain in Chapter 3.2).
It was achieved, that the optical table concept from the previous theses [13] and [14] is fully integrated into the test stand. A resolution of below 10 nm is realised (cf. Fig. 2.11) for the white LED's regime between 400 nm and 700 nm. A major change is the use of an acrylic cone instead of a two-lens system for coupling the light source into a fibre.
The light sources were designed to give the SiPM's p.d.e. over a broad spectrum, and a pulsed LED board including an amplifier for short light pulses delivering single photons was designed and built including seven monochrome LEDs.
A fully automised pre-characterisation can be carried out, leading to the SiPM's breakdown voltage and gives a precise start value for further measurements such as the p.d.e. or an SiPM's noise characteristics. The p.d.e. measurements are carried out automised and relative measurements are adjusted and rescaled to those of the absolute p.d.e.
The SiPMs breakdown voltage could be determined via I-V-line to have a voltage region for the measurements. Through the SiPM's relative gain, the breakdown voltage can be estimated more accurately. The former gives only a rough estimator to have a point of operation for the following measurements, the latter gives a higher accuracy of
$V_{\mathrm{BD}} = (69.72 \pm 0.01)$ V. The absolute p.d.e. could be measured with an accuracy

for each point of p.d.e.$_{407\,nm} = (19.7 \pm 1.0)\,\%$, p.d.e.$_{470\,nm} = (23.9 \pm 1.1)\,\%$ and p.d.e.$_{505\,nm} = (17.6 \pm 1.5)\,\%$. The data measured for the SiPM's relative p.d.e. can then be adjusted to this fir the absolute p.d.e., to have the SiPM's sensitivity in a region between 420 nm and 700 nm.
The whole measurements sequence takes less than an hour for the different characterisation steps of the SiPM. This and the above shows, that we now have an automised tool to characerise an SiPM's parameters in little time.

5. Outlook

To gain better knowledge of the sub 400 nm regime, one has to choose another wide spectrum light source as a substitution for the white light LED. The single wavelength LEDs in use still have the disadvantage of large FWHM values (cf. Fig. B.6 through B.8).
Furthermore, measurements were not carried out in a stabilised temperature environment, and a temperature regulation is already in development, its design will be adjusted to match the existing test stand. With this addition, temperature and wavelength dependent characterisations will be possible.
The SiPM preamplifier has on the one hand the advantage of giving inverted signals, but since it has not explicitly been developed for SiPM amplifying but only improved for an SiPM, a complete redesign might lead to improved relative p.d.e. measurements. This redesign would have to choose filters for the supply voltage carefully, that do not influence the SiPM current too much. Furthermore, the existing bandwidth of estimated $100 - 200$ MHz[1] should at least be doubled.
The tests for correlated noise can also be easily incorporated into the existing setup, giving information about an SiPM's noise-behaviour at different temperatures. For the noise measurements, one could also look further into what the oscilloscope is capable of, since it is already incorporated into the test stand and routines are being developed.

[1] Personal communication with electronic department

Bibliography

[1] Hamamatsu *MPPC datasheet*, Available at: <http://sales.hamamatsu.com/en/products/solid-state-division/si-photodiode-series/mppc/part-s10362-11-100c.php> [Accessed 22 May 2012].

[2] The CMS Collaboration, et al., 2008. The CMS experiment at the CERN LHC. *Journal of Instrumentation* [journal] 3 (S08004). Available through: IOPscience database [Accessed 22 May 2012].

[3] The Pierre Auger Collaboration, 2010. The fluorescence detector of the Pierre Auger Observatory. *Nuclear Instruments and Methods in Physics Research Section A: Accelerators, Spectrometers, Detectors and Associated Equipment* [journal] 620 (2-3), pp.227-251. Available through: Science Direct SciVerse database [Accessed 22 May 2012].

[4] Tully, C. et al., 2011. High-Speed Imaging Photo-Detection Systems. The Compact Muon Solenoid Experiment Detector Note CMS DN-2011/003. Available through: CMS information server.

[5] Niggemann, T., 2012. *New Telescope Design with Silicon Photomultipliers for Fluorescence Light Detection of Extensive Air Showers*. M. Sc. Phys. III. Phys. Inst. A, RWTH Aachen University.

[6] Renker, D. and Lorenz, E., 2009. Advances in solid-state photon detectors. *Journal of Instrumentation* [journal] 4, P04004. Available through: IOPscience database [Accessed 22 May 2012].

[7] Korpar, S., 2010. Status and perspectives of solid state photon detectors. *Nuclear Instruments and Methods in Physics Research Section A: Accelerators, Spectrometers, Detectors and Associated Equipment* [journal] 639 (1), pp.88-93. Available through: Science Direct SciVerse database [Accessed 22 May 2012].

[8] Cova, S. et al., 2003. Evolution and prospects for single-photon avalanche diodes and quenching circuits. *Journal of Modern Optics*, [online]. Available at: <http://risorse.dei.polimi.it/spad/2004/JMO2004.pdf> [Accessed 22 May 2012]

[9] Tadday A. et al., 2010. Characterisation studies of silicon photomultipliers. *Nuclear Instruments and Methods in Physics Research Section A: Accelerators, Spectrometers, Detectors and Associated Equipment*, 620(2-3). Available at: <http://arxiv.org/abs/1003.6071> [Accessed 22 May 2012].

[10] Lauscher M., 2012. *Characterisation Studies of Silicon Photomultipliers for the Detection of Fluorescence Light from Extensive Air Showers*. M.Sc. phys., III. Phys. Inst. A, RWTH Aachen University.

[11] Dolgoshein, B. et al., 2003. Silicon photomultiplier and its possible applications. *Nuclear Instruments and Methods in Physics Research Section A: Accelerators, Spectrometers, Detectors and Associated Equipment* [journal] 504 (1-3), pp.48-52. Available through: Science Direct SciVerse database [Accessed 22 May 2012].

[12] Dolgoshein, B. et al., 2001. An Advanced Study of Silicon Photomultiplier. *ICFA Instrumentation Bulletin*, [online]. Available at: <http://www.slac.stanford.edu/pubs/icfa/fall01/paper3/paper3.pdf> [Accessed 22 May 2012].

[13] Richer, S., July 2010. *Conception of a test stand for Silicon Photomultipliers*. B. Sc. phys. III. Phys. Inst. A, RWTH Aachen University.

[14] Lins, M., July 2010*Construction and testing of a tunable light source for characterisation of Silicon Photomultipliers*. B. Sc. phys. III. Phys. Inst. A, RWTH Aachen University.

[15] Hallen, P., 2011. *Determination of the Recovery Time of Silicon Photomultipliers*. B. Sc. phys. III. Phys. Inst. A, RWTH Aachen University.

[16] Setlur, A., 2009. Phosphors for LED-based Solid-State Lighting. *The Electrochemical Society*, [online]. Available at:

<https://electrochem.org/dl/interface/wtr/wtr09/wtr09_p032-036.pdf> [Accessed 22 May 2012].

[17] Schröder G. and Treiber H., 2007. *Technische Optik: Grundlagen und Anwendungen*.

[18] Schulte, J.-F., 2010. *Studies of SiPM properties using an integrating sphere*. B. Sc. Phys. III. Phys. Inst. A, RWTH Aachen University.

[19] OceanOptics, n.d. *The Ocean Optics Catalog of Products* [pdf], p.184. Available at: <http://www.oceanoptics.com/catalog/Ocean_Optics_Catalog_2012.pdf> [Accessed 22 May 2012].

[20] Keithley, *Model 2400 Sourcemeter User's Manual, 2400S-900-01 Rev. K / September 2011*. [manual] Available at: <http://www.keithley.de/data?asset=887> [Accessed 30 May 2012].

[21] CAEN *Technical Information Manual*, Revision n. 8, 15 July 2008, MOD. V965/V965A, 16/8 CHANNEL DUAL RANGE QDC.

[22] CAEN *Technical Information Manual*, Revision n. 5, 6 July 2011MOD. V 812 series 16 CH. CONSTANT FRACTION DISCRIMINATORS.

[23] ThorLabs, n.d. [image online] Available at: <http://www.thorlabs.com/catalogpages/V21/1014.PDF> [Accessed 22 May 2012].

[24] ThorLabs, n.d. [image online] Available at: <http://www.thorlabs.com/images/popupimages/NE510A.jpg> [Accessed 22 May 2012].

[25] ThorLabs, n.d. [image online] Available at: <http://www.thorlabs.com/images/TabImages/IS200%20Material%20Reflectance.jpg> [Accessed 22 May 2012].

[26] Keithley, *Model 6485 Picoammeter User's Manual, 6487-900-01 Rev. C / March 2011*. [image] Available at: <http://www.keithley.com/data?asset=15843> [Accessed 22 May 2012].

[27] ThorLabs, n.d. [image online] Available at:
<http://www.thorlabs.com/images/TabImages/AchromatACoating_300.jpg>
[Accessed 22 May 2012].

[28] ThorLabs, n.d. [image online] Available at:
<http://www.thorlabs.com/images/popupimages/A220_plt.gif>
[Accessed 22 May 2012].

A. Abbreviations

In alphabetical order

Amp. - amplifier
CFD - constant fraction discriminator
CMS - Compact Muon Solenoid
FWHM - full width at half maximum
G-APD - Geiger mode avalanche photo diode
HF - hadron forward
LED - light-emitting diode
LHC - Large Hadron Collider
ND filter - neutral density filter
abs./rel. p.d.e. - absolut/relative Photon Detection Efficiency
p.e. - photon equivalent
PIN diode - positive intrinsic negative diode
PMT - photomultiplier tube
QDC - charge-to-digital converter
QE - quantum efficiency
SiPM - Silicon photomultiplier
V_{BD} - breakdown voltage
V_{bias} - bias voltage
V_{OV} - overvoltage
VM-USB - VME master-USB
VME(bus) - versa module eurocard(bus)

B. Additional Figures

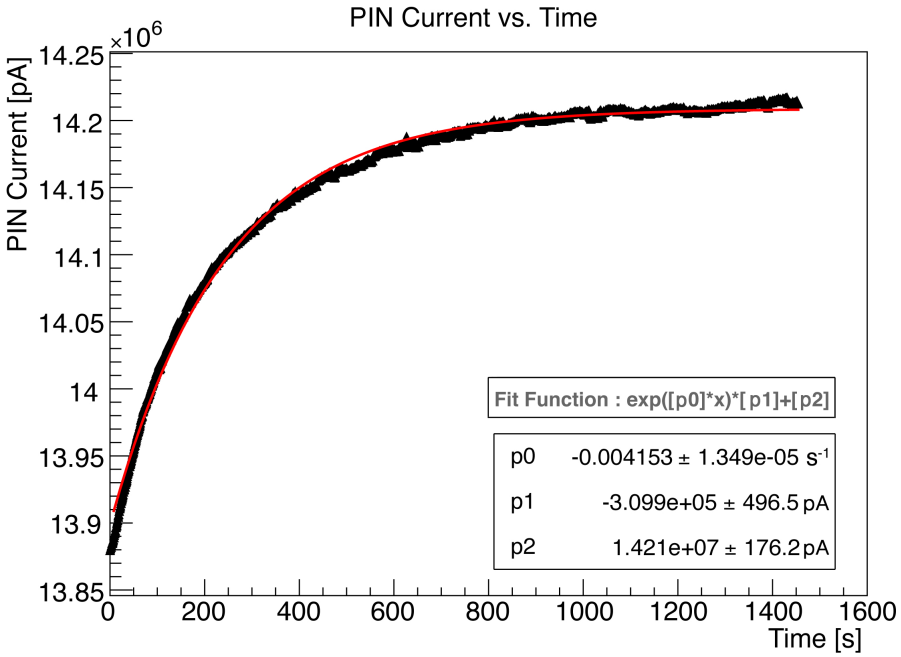

Figure B.1.: Picoammeter measurement of the PIN diode's current as the white LED current is instantaneously decreased from 600 mA until 500 mA.

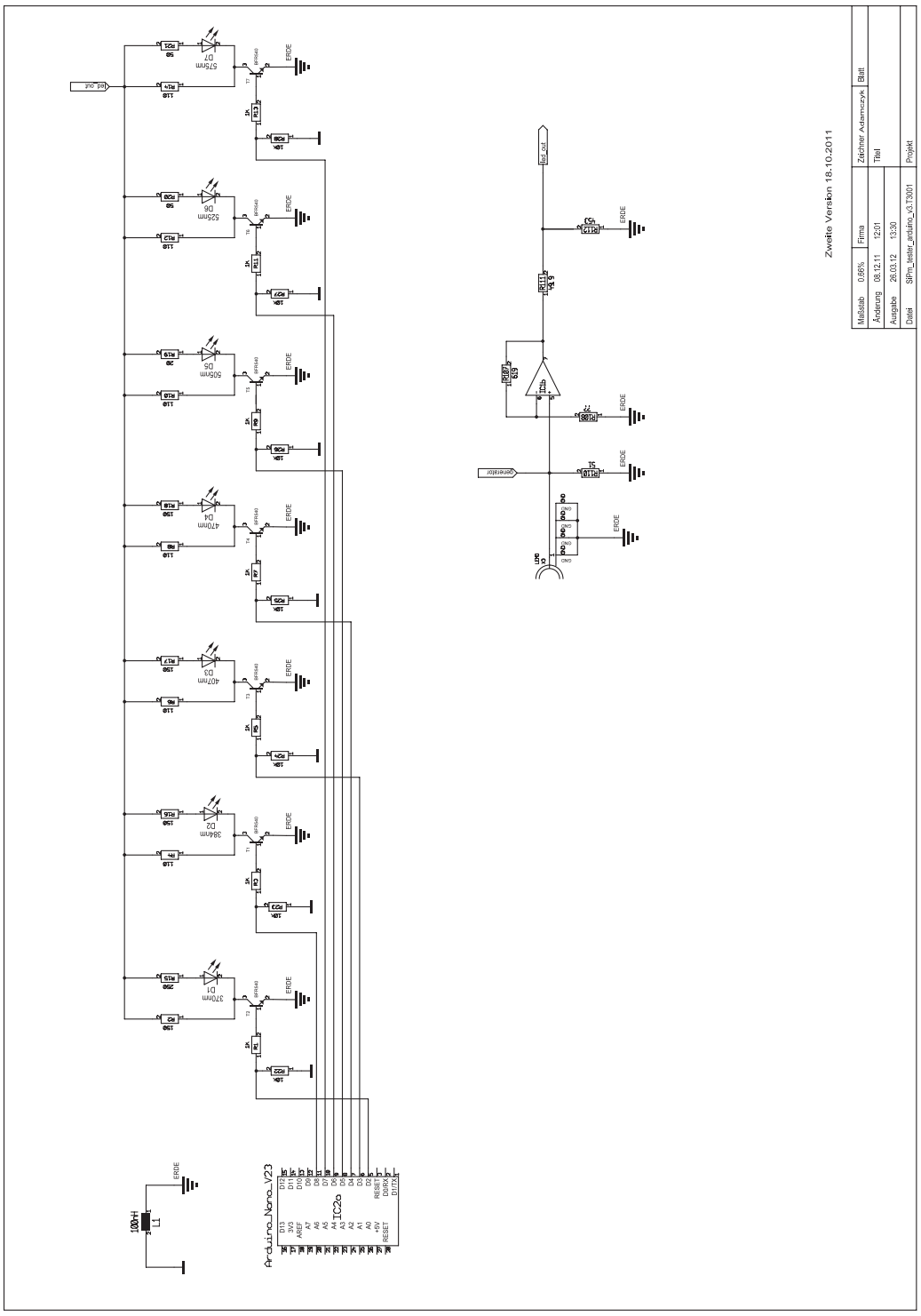

Figure B.2.: Circuit for the seven LED pulser board.[Drawing: Franz Adamczyk]

Figure B.3.: Spectrum of the 370 nm LED.

Figure B.4.: Spectrum of the 384 nm LED.

Figure B.5.: Spectrum of the 407 nm LED.

Figure B.6.: Spectrum of the 470 nm LED.

Figure B.7.: Spectrum of the 505 nm LED.

Figure B.8.: Spectrum of the 525 nm LED.

Figure B.9.: Spectrum of the 575 nm LED.

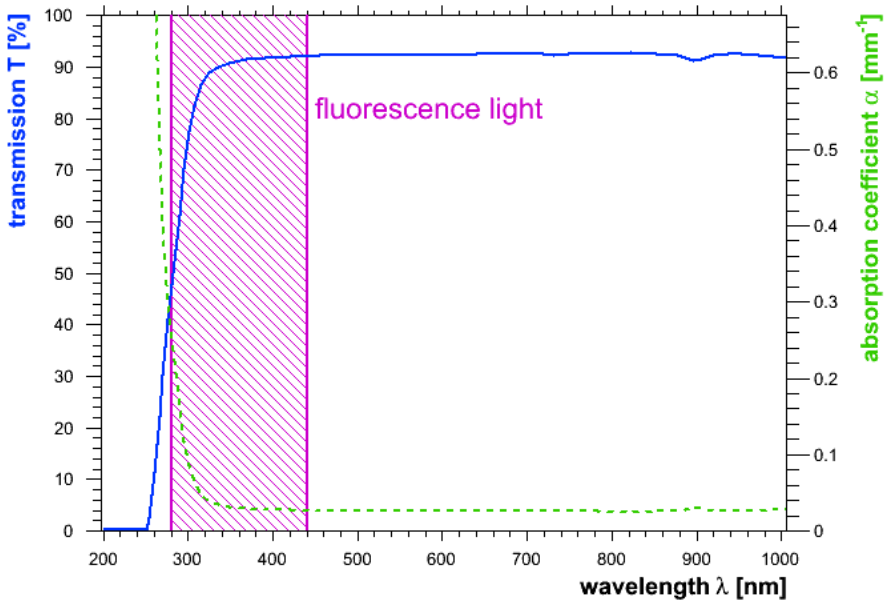

Figure B.10.: Transmission of PMMA material.[5]

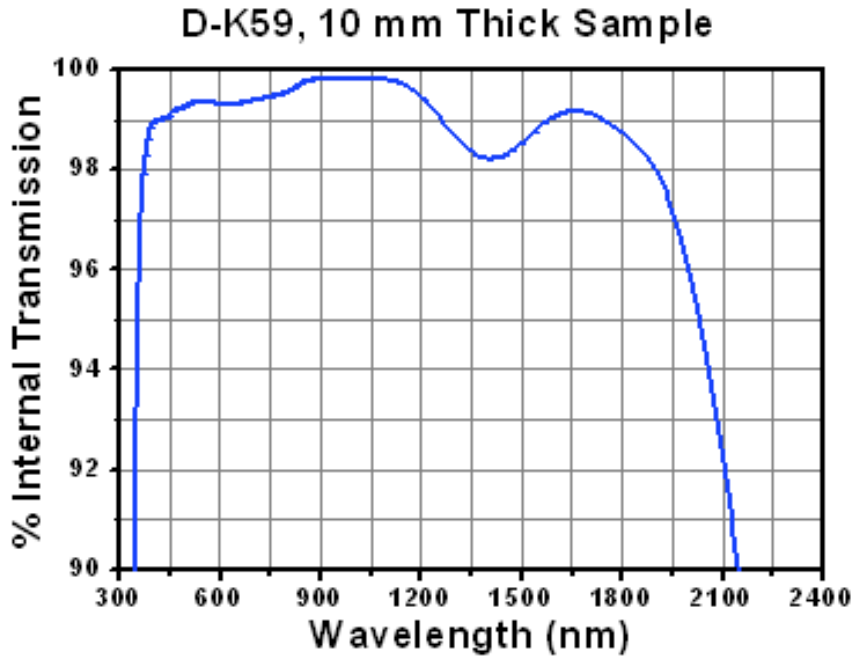

Figure B.11.: Transmission of D-K59 glass used for the first collimator lens.[28]

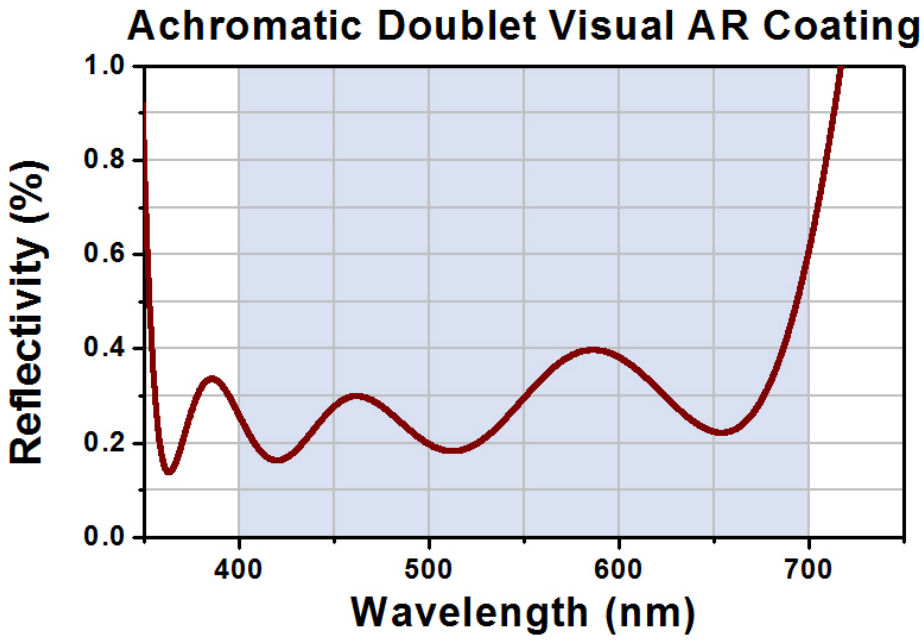

Figure B.12.: Reflectivity of the achromatic doublet used as second collimator lens.[27]

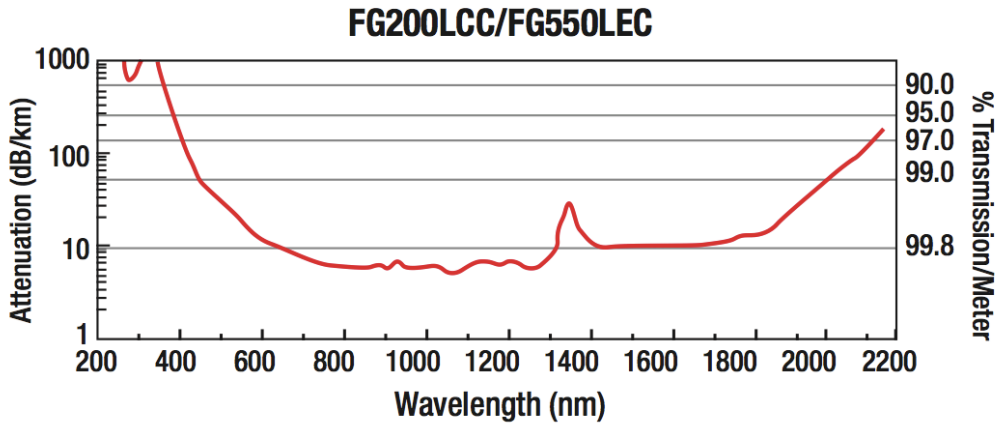

Figure B.13.: Attenuation curve for the used light-guide fibres.[23]

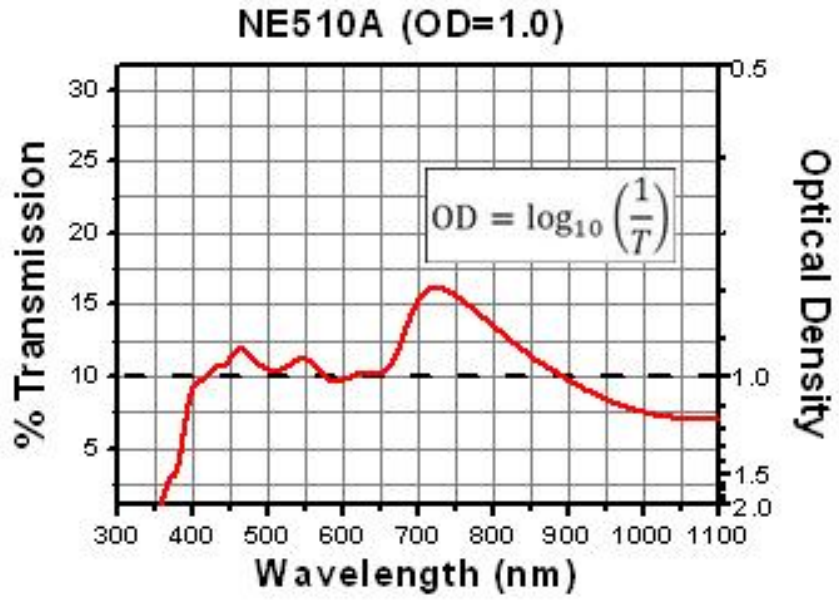

Figure B.14.: Transmission data for ThorLabs NE510A neutral density filter.[24]

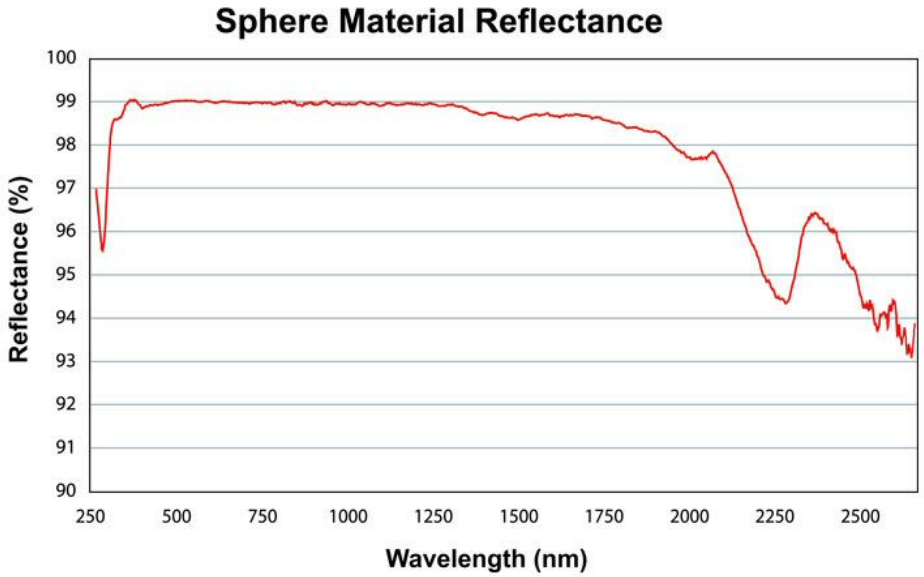

Figure B.15.: Reflectivity of the material on the inside of the integrating sphere (PTFE).[25]

RANGE	5½ DIGIT DEFAULT RESOLUTION	ACCURACY (1YR) [1] ±(% RDG. + OFFSET) 18°–28°C, 0–70% RH	TYPICAL RMS NOISE [2]	ANALOG RISE TIME [3] (10% to 90%)
2 nA	10 fA	0.4 % + 400 fA	20 fA	8 ms
20 nA	100 fA	0.4 % + 1 pA	100 fA	8 ms
200 nA	1 pA	0.2 % + 10 pA	1 pA	500 µs
2 µA	10 pA	0.15% + 100 pA	10 pA	500 µs
20 µA	100 pA	0.1 % + 1 nA	100 pA	500 µs
200 µA	1 nA	0.1 % + 10 nA	1 nA	500 µs
2 mA	10 nA	0.1 % + 100 nA	10 nA	500 µs
20 mA	100 nA	0.1 % + 1 µA	100 nA	500 µs

Figure B.16.: Specifications for Keithley Picoammeter 6485.([26], p. A1)

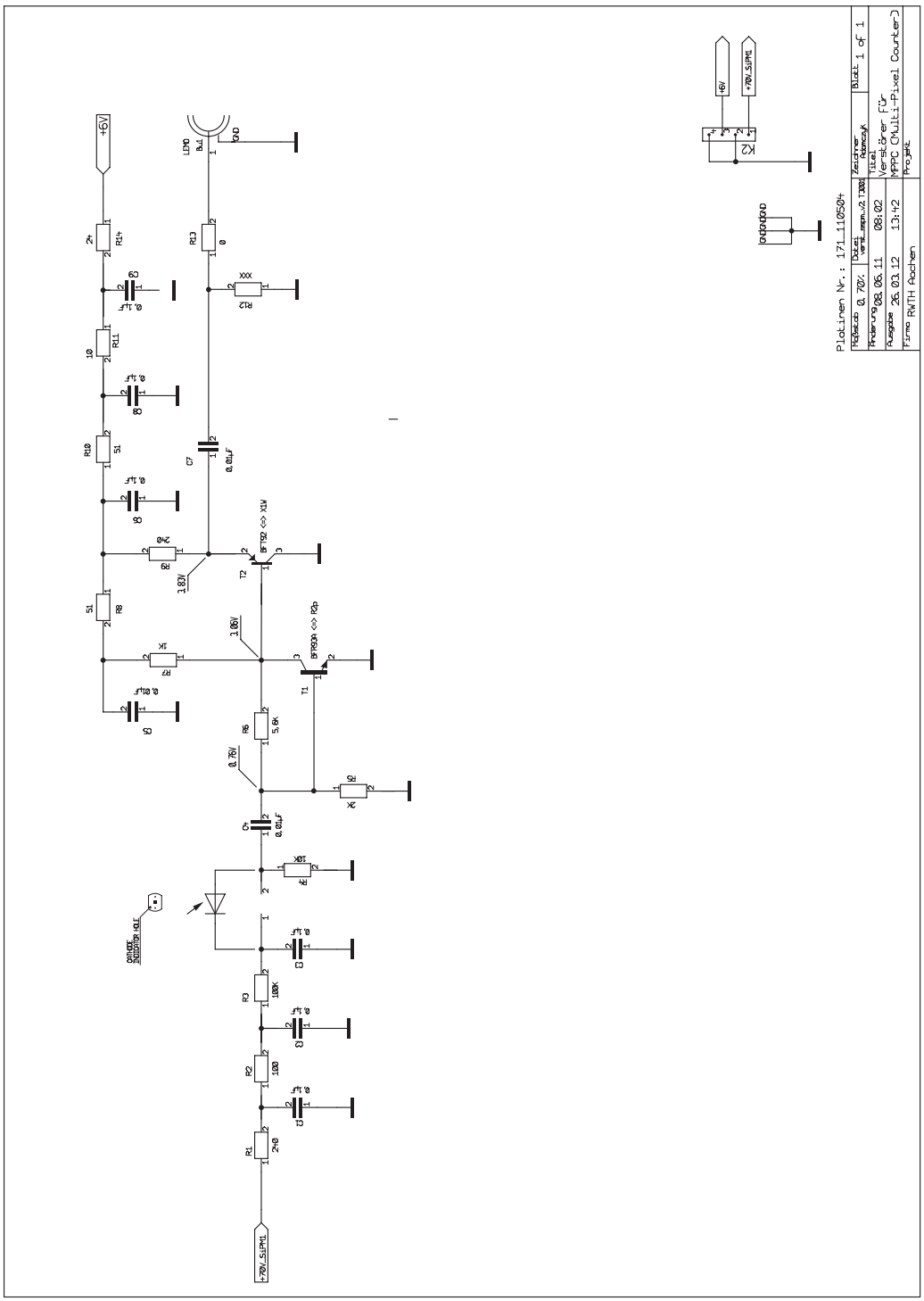

Figure B.17.: Electric circuit of the SiPM connector board and the preamplifier attached to the same board.[Drawing: Franz Adamczyk]

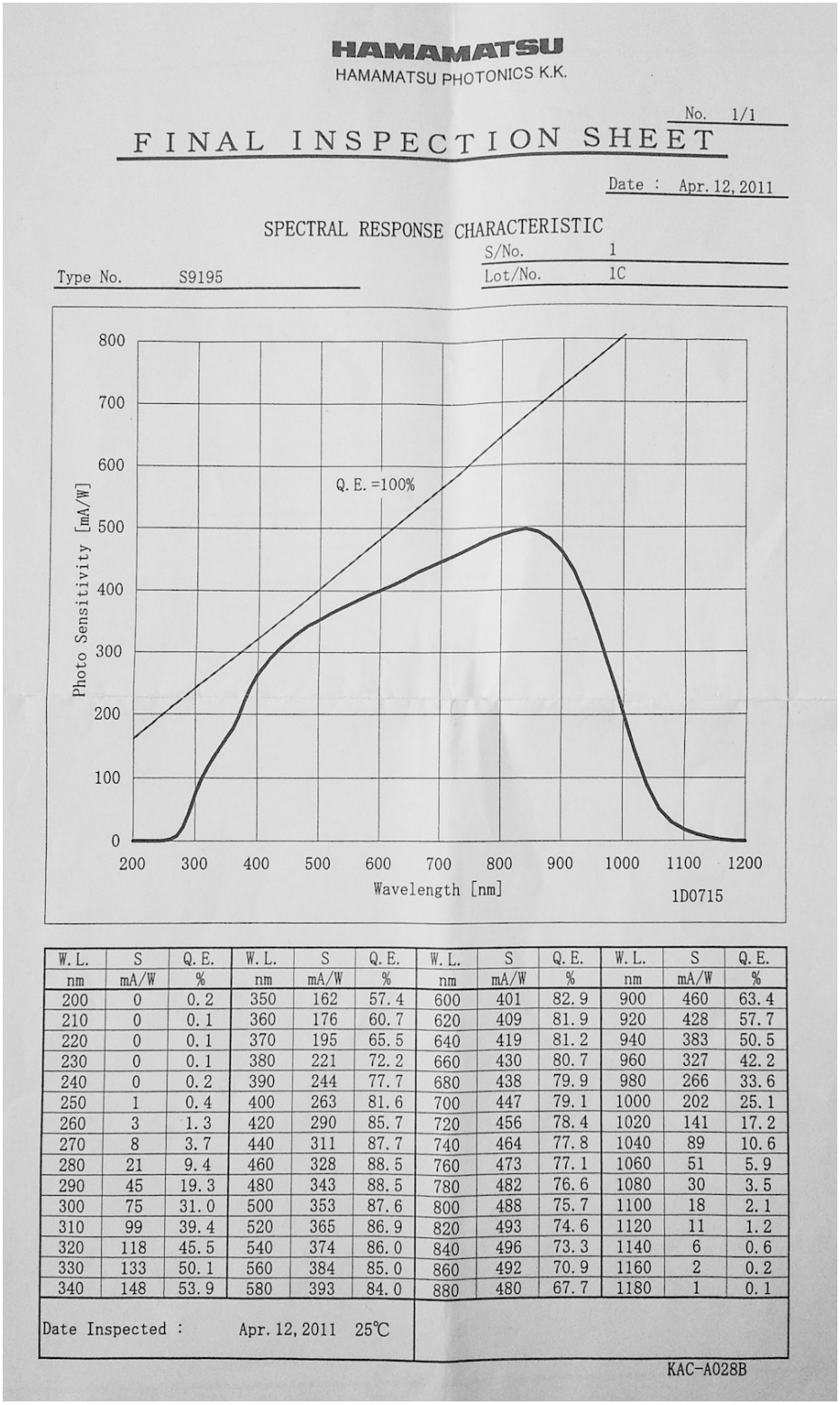

HAMAMATSU

HAMAMATSU PHOTONICS K.K.

No. 1/1

FINAL INSPECTION SHEET

Date : Apr. 12, 2011

SPECTRAL RESPONSE CHARACTERISTIC

S/No. 1

Type No. S9195 Lot/No. 1C

W.L. nm	S mA/W	Q.E. %	W.L. nm	S mA/W	Q.E. %	W.L. nm	S mA/W	Q.E. %	W.L. nm	S mA/W	Q.E. %
200	0	0.2	350	162	57.4	600	401	82.9	900	460	63.4
210	0	0.1	360	176	60.7	620	409	81.9	920	428	57.7
220	0	0.1	370	195	65.5	640	419	81.2	940	383	50.5
230	0	0.1	380	221	72.2	660	430	80.7	960	327	42.2
240	0	0.2	390	244	77.7	680	438	79.9	980	266	33.6
250	1	0.4	400	263	81.6	700	447	79.1	1000	202	25.1
260	3	1.3	420	290	85.7	720	456	78.4	1020	141	17.2
270	8	3.7	440	311	87.7	740	464	77.8	1040	89	10.6
280	21	9.4	460	328	88.5	760	473	77.1	1060	51	5.9
290	45	19.3	480	343	88.5	780	482	76.6	1080	30	3.5
300	75	31.0	500	353	87.6	800	488	75.7	1100	18	2.1
310	99	39.4	520	365	86.9	820	493	74.6	1120	11	1.2
320	118	45.5	540	374	86.0	840	496	73.3	1140	6	0.6
330	133	50.1	560	384	85.0	860	492	70.9	1160	2	0.2
340	148	53.9	580	393	84.0	880	480	67.7	1180	1	0.1

Date Inspected : Apr. 12, 2011 25℃

KAC-A028B

Figure B.18.: Datasheet for calibrated PIN diode Hamamatsu S9195.

List of Figures

1.1. A Hamamatsu SiPM, Model S10362-100C with 900 pixels and (1x1) mm^2 active area (Photo: Benjamin Glauß, 2012). 1

1.2. Simplified schematic depiction of a p-on-n type G-APD (Benjamin Glauß, 2012). 2

1.3. Electric scheme for a single SiPM pixel denoting the components that account for a pixel's electrical behaviour (Benjamin Glauß, 2012). 4

1.4. Size comparison between a Photomultiplier Tube on the left and the SiPM as in Fig. 1.1 (Photo: Benjamin Glauß, 2012). 4

1.5. Schematic depiction of a crosstalk event in two neighbour cells [8]. 5

1.6. SiPM pulses showing different effects and an example for a 0.5 p.e. pulse height. The scope's resolution is set to 100 mV/div, the time resolution is set to 20 ns/div. 5

1.7. Different SiPM pulses heights, representing the different charge amounts released in a breakdown for 1, 2, 3,... pixels. The trigger level is set to $V_T = -240$ mV. 6

1.8. P.d.e. for a Hamamatsu Silicon Photomultiplier [1]. 7

2.1. Schematic depiction of the light from the source being fanned out in the monochromator and coupled into the integrating sphere. . 10

2.2. Photograph of the optic table, showing the different components. The white LED is at position 1. The cone is inside the black tube at 2. The condenser is inside the tubes at 3. A shutter to screen the light is attached to the condenser tube at 4 a and controlled by a microchip at 4 b. The grating is at position 5. The pickup is at 6 a and moved by a DC servo motor at 6 b. The integrating sphere is at 7, where the SiPM (8) and the PIN diode are attached to. . . 11

2.3. White light LED consisting of short wavelength LED at the bottom surrounded by a phosphorous substance, the resulting white light LED's spectrum is shown above (Benjamin Glauß, 2012). . 13
2.4. At time $t = 0$ the white LED is switched on. The PIN diode measures a current (y-axis) that is proportional to the LED's light flux. 14
2.5. LED board housing seven monochromatic LEDs, electric components and cabling for pulsed operation (Photo: Benjamin Glauß, 2012). 15
2.6. Acrylic cone used to couple the different extended light sources into a fiber. Below is a simulated cone, done in Zemax (Photo: Benjamin Glauß, 2012). 16
2.7. Two stage collimator with an aperture, used to create a plane wave (Benjamin Glauß, 2012). 17
2.8. Calibration data for the neutral density filter ND1.0. 19
2.9. Single spectrum recorded with the spectrometer for calibration purposes 21
2.10. Calibration pickup position to wavelength (above), and the corresponding residua (below). 22
2.11. FWHM distribution for the different wavelengths where the light was picked up at. 23
2.12. SiPM connector board with SiPM holder and SiPM attached to the holder (Photo: Benjamin Glauß, 2012). 25

3.1. Schematic depiction of the setup for an SiPM pre-characterisation. Note the three consecutive steps for the three measurements included. 28
3.2. Gate (yellow) preceding the SiPM signal (pink) by 15 ns. The gate triggers the QDC recording, integrating the signals inside of the gate (de facto the vertical white lines). 29
3.3. I-V-Line for a Model S10362-100C Hamamatsu SiPM. 30
3.4. Threshold function for a Model S10362-100C Hamamatsu SiPM. The solid lines in b) are the parabolic fits for determining the 1 p.e. distance. 32
3.5. Single QDC spectrum for a Model S10362-100C Hamamatsu SiPM, showing the different photon equivalent peaks. 34
3.6. Threshold function for a Model S10362-100C Hamamatsu SiPM. 35

3.7. High statistics QDC spectrum for a Model S10362-100C Hamamatsu SiPM. 36
3.8. Peak width analysis for peaks in Fig. 3.7, using different fit widths. The red line shows the fit for 1.5σ, the grey lines for 1σ and 2σ respectively. 38
3.9. Setup for p.d.e. measurements. For relative p.d.e. determination, the upper light source is used (white LED, fanned out spectrum through grating, movable light pickup for picking up different wavelengths), absolute measurements with the light source below(pulsed LEDs). 39
3.10. Evaluation of PIN diode currents behind the integrating sphere, measured with a picoammeter. a) shows the raw current, b) shows the dark current, c) shows the difference between the values in a) and b), d) shows the photon count, incorporating the PIN diode's sensitivity. 41
3.11. Evaluation of SiPM currents behind the integrating sphere, measured with a sourcemeter. a) shows the raw current, b) shows the dark current, c) shows the difference between the values in a) and b), d) shows the sensitivity data from c) divided by that from 3.10c), not corrected for the ND filter. 42
3.12. P.D.E. values for a Model S10362-100C Hamamatsu SiPM, showing its relative behaviour in the visible spectrum. 43
3.13. QDC dark reference spectrum, no light coupled into the integrating sphere. 46
3.14. QDC spectrum for a pulsed LED with 407 nm 47
3.15. QDC spectrum for a pulsed LED with 470 nm. 48
3.16. QDC spectrum for a pulsed LED with 505 nm. 49
3.17. Combined results for the absolute and relative p.d.e. values at an over voltage of 79.72 V for a 100 pixel SiPM, Model S10362-100C. 49

B.1. Picoammeter measurement of the PIN diode's current as the white LED current is instantaneously decreased from 600 mA until 500 mA. 61
B.2. Circuit for the seven LED pulser board.[Drawing: Franz Adamczyk] 62
B.3. Spectrum of the 370 nm LED. 63
B.4. Spectrum of the 384 nm LED. 63
B.5. Spectrum of the 407 nm LED. 64

B.6. Spectrum of the 470 nm LED. 64
B.7. Spectrum of the 505 nm LED. 65
B.8. Spectrum of the 525 nm LED. 65
B.9. Spectrum of the 575 nm LED. 66
B.10. Transmission of PMMA material.[5] 66
B.11. Transmission of D-K59 glass used for the first collimator lens.[28] 67
B.12. Reflectivity of the achromatic doublet used as second collimator lens.[27] 67
B.13. Attenuation curve for the used light-guide fibres.[23] 68
B.14. Transmission data for ThorLabs NE510A neutral density filter.[24] 68
B.15. Reflectivity of the material on the inside of the integrating sphere (PTFE).[25] 69
B.16. Specifications for Keithley Picoammeter 6485.([26], p. A1) . . . 69
B.17. Electric circuit of the SiPM connector board and the preamplifier attached to the same board.[Drawing: Franz Adamczyk] 70
B.18. Datasheet for calibrated PIN diode Hamamatsu S9195. 71

Danksagungen An dieser Stelle möchte ich den Personen danken, ohne welche diese Arbeit nicht möglich gewesen wäre.
Dazu gehören vom Institut zu allererst Herr Professor Hebbeker, unter dessen kritischem Auge ich dazu kam, Fragen zu stellen und zu beantworten, welche ich sonst nicht gestellt hätte. Mein Betreuer, Dr. Markus Merschmeyer war ein ständiger Ansprechpartner, der mit deiner Detailverliebtheit auch noch so kleine Schwächen aufgedeckt hat und stets mit Rat und Tat zur Seite stand. Meinem Bürokollegen Carsten Heidemann muss ich dafür danken, mir in Fragen der Programmierung stets eine Hilfe gewesen zu sein und auch sonst offen für jegliche Fragen gewesen zu sein, genau wie Markus Lauscher, der mit seinem Wissen auf dem Gebiet der SiPMs eine ebenso große Hilfe war. Natürlich gilt mein Dank auch der mechanischen Werkstatt und Herrn Barthel Philipps, sowie der elektronischen Werkstatt und Herrn Franz Peter Zantis sowie Franz Adamczyk, um viele Bauteile meiner Arbeit zu diskutieren und zu realisieren.
Auf der anderen Seite bin ich auch meinem privaten Umfeld zu Dank verpflichtet. Meine Eltern und mein Bruder haben mich stets unterstützt in den Jahren meines Studiums. Genau so wie meine Freunde, auf welche ich mich verlassen konnte und kann, egal wie kurz oder lang ich sie auch kenne.

I assure hereby that this thesis is written autonomously by me, and that no further help was acquired than mentioned as a source or quotation.

Aachen, 31.03.11